

Effects of urban areas on the diurnal cycle of temperature and precipitation in a global climate simulation

Jack Katzfey¹ | K. Heinke Schlünzen² | Peter Hoffmann³

¹Environment, CSIRO, Aspendale, Victoria Australia

²Meteorol. Inst., Universität Hamburg, Germany

³Climate Service Center Germany (GERICS), Helmholtz-Zentrum hereon GmbH, Hamburg, Germany

Correspondence

Jack Katzfey, CSIRO, PMB 1, 107 Station Street, Aspendale, VIC, 3195, Australia.
 Email: jack.katzfey@csiro.au

Funding information

Helmholtz Institute for Climate Service Science (HICSS); Deutsche Forschungsgemeinschaft, Grant/Award Number: EXC177; German Federal Ministry of Education and Research (BMBF), Grant/Award Number: 01LN2204A; Germany's Excellence Strategy-EXC 2037, Grant/Award Number: 390683824

Abstract

Analyses of global climate model results for urban impacts on temperature and precipitation are rare. Previous analyses of the global Conformal Cubic Atmospheric Model simulation results for 1985–2010 have revealed urban effects on minimum and maximum temperatures. Using the same dataset to derive time-zone-corrected three-hourly local time period (LTP) data, averaged diurnal cycles of temperature and precipitation were calculated for grid cells with greater than 10% urban fraction (urban grid cells) globally. Three latitudinal bands were assessed: northern extratropics (NET, 274 urban grid cells), southern extratropics (SET, 39 urban grid cells), and the Tropics (26 urban grid cells). The largest statistically significant urban influences on temperature are consistently found at night, in agreement with many previous studies on urban heat islands. Signs of urban cooling were found for a few hours, from 09:00 to 15:00 LTP, most often in summer. Influences of urban areas on precipitation varied, with small increases and decreases in all latitudinal bands and seasons. For NET, increases were generally found. In the Tropics, increases were found from 21:00 to 09:00 LTP for all seasons except DJF, with decreases for all seasons from 15:00 to 18:00 LTP. In SET, all seasons had increases for 21:00 to 00:00 LTP and decreases for 15:00 to 18:00 LTP. DJF had decreases for all LTPs except 21:00 to 00:00 LTP and SON had increases for all times except 15:00 to 18:00 LTP. Differences in rainfall in the region surrounding the urban areas were broadly similar to local changes in NET. For the Tropics and SET, regional decreases were found for DJF and JJA, with a more varied pattern for other months. Regional effects appeared to be more restricted to near-urban areas in the Tropics than in NET. The results indicate some influence of nearby urban areas on regional temperature and precipitation.

KEY WORDS

Climate, diurnal, high-resolution, numerical model, urban influences

1 | INTRODUCTION

Urban areas with their high population density, industrial facilities and traffic account for 67%–72% of the world's greenhouse gas emissions (excluding aviation, shipping, and biogenic sources; IPCC, 2022a) and thereby contribute to global climate change. In addition, the urban fabric and its properties (albedo, heat storage, vertical extension) influence atmospheric variables. Vertically extended urban structures create a heterogeneous canopy layer, which influences the exchange processes between surfaces and atmosphere. In addition, human activities result in emissions of heat (i.e., anthropogenic heat) and a range of pollutants. Thus, urban areas generate unique atmospheric conditions, commonly known as urban climate (Oke *et al.*, 2017). The best-known urban climate phenomenon is the urban heat island effect (UHI), which is mainly revealed by higher nighttime temperatures in urban areas compared to their rural surroundings (WMO, 2023). The UHI was extensively investigated at the local, meso and regional scale (for scales see table 2.1 in WMO, 2023), and some studies have investigated the urban influence on temperature at the global scale (Hertwig *et al.*, 2021; Katzfey *et al.*, 2020; Oleson & Feddema, 2020). Katzfey *et al.* (2020) investigated the impact of urban areas on a range of atmospheric variables by running global climate simulations with the Conformal Cubic Atmospheric Model (CCAM; McGregor & Dix, 2008) at a 50-km global resolution. By employing the urban parameterization Urban Climate and Energy Model (UCLEM; Chapman *et al.*, 2018; Lipson *et al.*, 2017; Luhar *et al.*, 2014; Thatcher & Hurley, 2012), they found a UHI signal, as well as impacts on the regional and global temperature distribution. The mean, maximum, and minimum temperature data were analyzed, with the strongest increasing signal for the daily minimum temperature and almost no urban signal for the daily maximum temperature, reflecting to some extent the diurnal cycle of the UHI effect. However, the largest UHI effect does not necessarily occur at the same time as the daily temperature minimum. To have a more complete picture of the urban effect on temperature, an analysis of the diurnal temperature cycle is required. Hertwig *et al.* (2021) analyzed the UHI of London and Shanghai in the 10-km global simulations conducted with HadGEM3, which employs a bulk urban scheme, and compared it to hourly temperature observations for London and three-hourly observations for Shanghai. They found that the modeled UHI underestimated nighttime temperatures and that the diurnal cycle of urban temperature was shifted later compared to observations. Bohnenstengel *et al.* (2014) mention an increase in the nighttime planetary boundary layer height due to anthropogenic heat in London.

In addition to the urban temperature effect, cities also influence moisture variables (e.g., relative humidity decreases; Langendijk *et al.*, 2019) and rainfall (e.g., Han *et al.*, 2014; Liu & Niyogi, 2019; Schlünzen *et al.*, 2010). This is of special importance for city planners because not only high temperatures but also climate-change-related precipitation changes are already posing a hazard for urban areas in most parts of the world, for example by increased flooding due to extreme precipitation (IPCC, 2022b). Observational and modeling studies often show that there is an urban impact on precipitation (UIP). The impact can be caused by a combination of different effects (Han *et al.*, 2014): (i) thermally induced circulation between urban and rural areas caused by the UHI effect; (ii) emissions of particles from urban sources that affect the cloud microphysics (e.g., act as additional cloud condensation nuclei); (iii) reduced wind speeds over urban areas due to higher roughness, which leads to a convergence above urban areas; (iv) updrafts potentially enhancing convection and downwind precipitation. While the UIP studies mainly refer to the enhancement of precipitation and in particular convective precipitation downwind of urban areas, there are also studies that show a downwind suppression of precipitation (Donmez *et al.*, 2022; Xiao *et al.*, 2021). The impact of altering cloud microphysics by pollutants is the increase or suppression of rainfall, depending on the background concentration of aerosols, the size and type of the aerosols and gases emitted from the urban area, and type of convective system. Furthermore, there is also a complex interplay of the urban effects with mesoscale and regional circulation systems such as land-sea breeze circulation, mountain valley winds, monsoonal systems and surrounding orography (e.g., Fan *et al.*, 2020; Kusaka *et al.*, 2019; Paul *et al.*, 2018). This makes it challenging when investigating urban influences on precipitation globally, where several factors are combined, and mesoscale effects are averaged out. For instance, Chen and Frauenfeld (2016), who investigated the impact of urban areas on precipitation with a regional climate model, stated that urbanization effects "are due to the combined effects of both local moisture changes and large-scale circulation features." Georgescu *et al.* (2021) showed in modeling studies for the USA that urbanization needs to be included in order to determine future changes in precipitation extremes, and that urbanization can both suppress and increase precipitation. Other long-term modeling studies found only weak urban impact on the climatological mean (e.g., Daniel *et al.*, 2019), though these studies were only focused on specific regions such as the United States and Europe.

The global analysis based on 50-km global CCAM simulations conducted by Katzfey *et al.* (2020) did not reveal a UIP on the long-term annual precipitation, given the

large climate variability in rainfall. However, other studies found a UIP mainly for summertime rainfall (Liu & Niyogi, 2019), which is mostly convective-driven and has a clear diurnal cycle. Hence, a more detailed analysis taking into account diurnal and seasonal variation might detect an urban signal. Since the CCAM simulations did show an urban impact on temperature (UIT), the thermodynamics above urban areas were altered and the wind speeds reduced by the roughness effect of urban areas, which might influence precipitation formation in the model. However, given the quite coarse resolution of 50 km in the simulations, mesoscale circulations cannot be fully resolved. In addition, effects due to possible aerosol changes on cloud microphysics are not included in the simulations, which might alter the UIP.

The focus of the current paper is on assessing mean urban influences on the diurnal cycle of temperature and precipitation by season and latitudinal bands for the current climate, using data extracted from global simulations and averaging over many cities to determine regional and local effects. The following research questions are investigated:

- What is the local urban influence on the diurnal cycles of temperature and precipitation? Does it depend on season and latitudinal band (tropical/extratropical areas)?
- What is the regional urban influence on the diurnal cycles of temperature and precipitation? Does it depend on season and latitudinal band (tropical/extratropical areas)?

Section 2 of this paper discusses the methodology, including the datasets used in this paper and the model, CCAM, used to create them. Methods are introduced to extract (a) diurnal cycles (Section 2.2) and (b) urban impacts (Section 2.3) from global model results. In addition, a method to generate composites centered on urban grid cells (grid cells with urban fraction greater than 10%) to determine their regional effects is presented in Section 2.4 and the method used to calculate statistical significance in Section 2.5. In Section 3 the diurnal signals of temperature and precipitation are analyzed globally. In Section 4, urban influences on the diurnal cycle are studied from local to regional scales. Finally, results are summarized and discussed, and conclusions are drawn in Section 5.

2 | METHODOLOGY

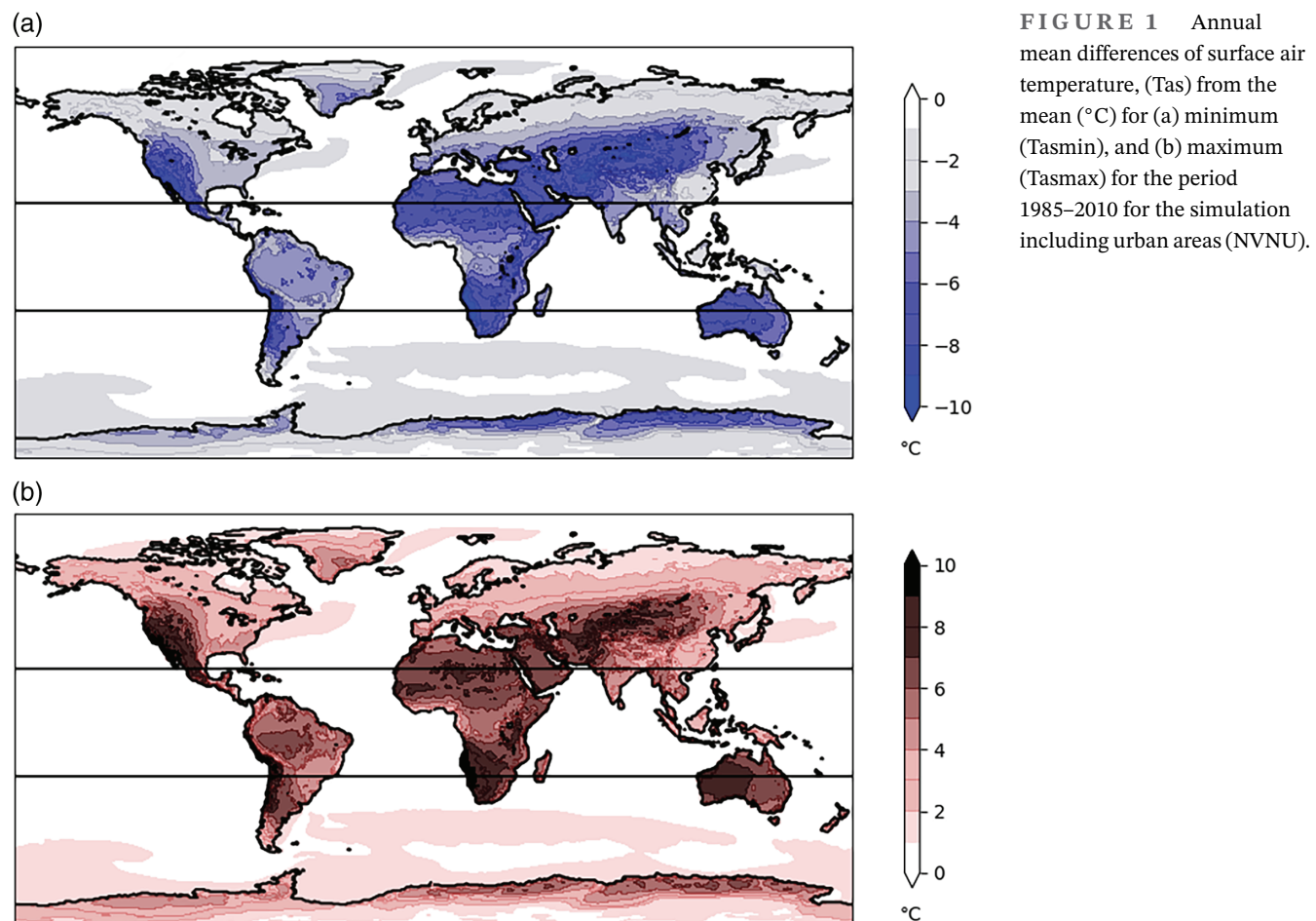
The model and datasets used to investigate the impact of urban areas on temperature and precipitation are

described in this section, as well as analysis techniques employed. The model results have been previously analyzed in Katzfey *et al.* (2020) with respect to the land cover influences on minimum and maximum temperatures and are further analyzed in this study to determine urban impacts on temperature and precipitation and the diurnal cycles of both.

2.1 | Dataset used

Results of the CCAM (McGregor & Dix, 2008) are used in this study for investigating the impact of urban areas on local (grid cell scale, see end of this section), regional and global climate. CCAM is an open-source global stretched-grid non-hydrostatic numerical model, which has been extensively used for regional climate studies (e.g., Grose *et al.*, 2015; Katzfey *et al.*, 2016; Thevakaran *et al.*, 2016) and has provided data to CORDEX (e.g., Di Virgilio *et al.*, 2019). Both the reanalysis-driven and the historical SST-only-driven global 50-km simulations show a good performance for temperature and rainfall compared to other climate models (e.g., Di Virgilio *et al.*, 2019; Evans *et al.*, 2021). CCAM includes a comprehensive set of physical parameterizations, including the Geophysical Fluid Dynamics Laboratory parameterizations for long-wave and short-wave radiation (Freidenreich & Ramaswamy, 1999; Lacis & Hansen, 1974; Schwarzkopf & Ramaswamy, 1999). The interactive cloud distributions are determined using the liquid- and ice-water scheme of Rotstayn (1997). Direct and indirect effects of sulfate aerosols are considered following Rotstayn and Lohmann (2002). An updated version of the McGregor (2003) convection scheme is used. In addition, CCAM employs a state-of-the-art urban parameterization based on the Town Energy Budget approach (TEB; Masson, 2000), denoted here as UCLEM (Thatcher & Hurley, 2012), which is coupled to the Community Atmosphere Biosphere Land Exchange model (CABLE) land surface scheme (Kowalczyk *et al.*, 2006). UCLEM is an urban canyon model that performed well in an intercomparison study of urban parameterizations (Lipson *et al.*, 2024). Note that the selected urban parameters were fixed globally (e.g., building height, albedo) but their influence depends on the urban fraction. The anthropogenic heat flux is dynamically calculated within UCLEM; it can vary for every time step and grid cell of the model. See section 2.2 in Katzfey *et al.* (2020) for more details of the model setup.

All simulation results presented here and used in Katzfey *et al.* (2020) were produced using CCAM with a C192 cubic grid (where each of the six sides of the cube have 192 × 192 grid cells) with approximately 50-km global resolution (see Figure 1 in Katzfey *et al.*, 2020) and



27 vertical layers. The lowest layer was 22 m above the displacement height. Note that data from the raw CCAM grid is interpolated to a 0.5° longitude by 0.5° latitude grid for analysis. The analyses in Katzfey *et al.* (2020) focused on the influences of urban parameterization and prescribed surface cover on global climate simulation results. In the present paper, we use the same dataset with a focus on diurnal cycles of temperature and precipitation using the greenhouse gas and aerosol emissions specified in the historical period from 1980 until 2005 and using the RCP8.5 scenario (Meinshausen *et al.*, 2011) until the end of the climate simulations in 2010.

Resolving urban areas is a challenge in global climate models (GCMs) due to their coarse resolution, thus urban parameterization is essential. As noted in Katzfey *et al.* (2020) and others (e.g., Daniel *et al.*, 2019; Qian *et al.*, 2022), there is growing evidence that urban areas are influencing both the local and regional climate. Another issue in GCMs is obtaining high-quality global input data for urban land cover. As in Katzfey *et al.* (2020), the land cover dataset used in this study was from MODIS¹ (Friedl *et al.*, 2010; Friedl & Sulla-Menashe, 2015), with a

resolution of about 5 km, based upon data for 2012. Note we keep the urban fraction fixed at this value throughout the simulation (1980 to 2010), that is, no urbanization (change in urban fraction) is included. While an updated and time-varying dataset could be used, it would complicate the interpretation of the results.

Land use data from MODIS are labeled “NV” (New Vegetation) and the urban data are labeled “NU” (New Urban), to be consistent with the previous study (Katzfey *et al.*, 2020). The run NVNU includes NV (vegetated and non-vegetated land uses) as well as NU (urban areas), while the run NV considers non-urban land use only. Within CCAM, up to five land use types can be specified (including bare soil) for each grid cell plus the urban fraction. A grid cell can be either land or water (no partial water is allowed in a grid cell). To make the code run more efficiently, only urban fractions greater than 1% of the grid cell area were used for inputs to the simulations presented here, with values below 1% set to zero.

The input datasets for the non-urban experiments (NV) were created by filling the NVNU CCAM urban portion of grid cells with the non-urban land cover types of that same

grid cell, keeping the relative fraction of each of the five land use types fixed to represent the “natural” surrounding land use instead of replacing urban areas with bare soil. This is possible because every grid cell in the NU dataset had less than 100% urban fraction (the maximum value was 89% for Tokyo). For example, if a NVNU grid cell had values of 50% urban, 25% bare soil and 25% shrubs, the NV land use would be 50% bare soil and 50% shrub.

For analyses of the current climate, averages from 1985 to 2010 were used; the period from 1980 to 1984 was deemed as the spin-up period and was not included in subsequent analyses. Analysis (not shown) indicated that soil properties (temperature and moisture) have stabilized before the end of the five-year spin-up period (see Katzfey *et al.*, 2020 for additional discussion). Note that both simulations (NVNU and NV) used the same sea surface temperatures; thus, differences in the large-scale internal variability are reduced. While local internal variability still exists, to some extent the internal variability will be reduced by averaging results over 26 years and many urban grid cells per latitudinal band when comparing the two simulations.

As mentioned, the dataset comes with a grid cell size of about 50 km, so urban areas are subgrid scale. Analyses of local influences, that is, for distances of 300 m to 2 km (Table 2.1 of WMO, 2023), are not possible. The smallest-scale changes assessed in this paper are changes in the atmosphere at grid cell scale. Despite its much larger extension (~50 km), this is considered to be *local scale* here. *Regional scale* is defined in this paper to be the 5°–5° longitude–latitude region surrounding the urban areas.

2.2 | Determination of diurnal cycle

Since one of the key interests of this study is the impact of urban areas on the diurnal signal, the data were reorganized into local time periods (LTP) globally (i.e., by collecting all 00:00 LTP data from around the globe into one

dataset). Model data were available at three-hourly intervals for surface air temperature (Tas), surface zonal wind (Uas), surface meridional wind (Vas) and three-hourly accumulated precipitation (Pr). In addition to Tas, Uas, Vas and Pr with their diurnal cycles, daily maximum (Tasmax) and minimum (Tasmin) temperatures were used.

Since model data are saved for three-hourly time periods, it is only possible to create eight longitudinal LTP bands in a day. To collect the global data corresponding to a given LTP, 45° wide longitudinal bands were introduced and related to the corresponding three-hourly UTC times as shown in Table 1. Thus, global data attributed to a midnight LTP (00:00 LTP) are the combination of the 00:00 UTC/−22.5° to 22.5° longitude band with the 03:00 UTC/22.5° to 67.5° longitude band, continuing along the diagonal in the table, to provide a global map of data at 00:00 LTP. This allocates data at different UTC times to a given LTP. Analysis indicated that average values were not significantly affected by values at the edges of longitudinal bands (Section 3). Note that for precipitation the three-hour accumulation interval ends at the given LTP. Global data compiled by the above method for each LTP are combined into one time series for each LTP over the multiyear time period (1985–2010). Means for each LTP are then computed seasonally and annually. The standard deviation is computed over time and then averaged over all urban grid cells for a given LTP and season.

2.3 | Determination of urban impacts

In this study, urban impacts on air temperature and precipitation (and surface air humidity and winds, presented in the Supplementary information) were calculated by subtracting the runs with (NVNU) and without (NV) urban areas (NVNU – NV). All parameters considered were grid cell values. For the run with urban areas (NVNU), the grid cell values are the combination of the weighted urban

TABLE 1 Local time period (LTP) in relation to universal time code (UTC) and longitude band.

UTC	Longitude bands							
	−22.5°–22.5°	22.5°–67.5°	67.5°–112.5°	112.5°–157.5°	157.5°–202.5°	202.5°–247.5°	247.5°–292.5°	292.5°–337.5°
0000	00:00	03:00	06:00	09:00	12:00	15:00	18:00	21:00
0300	03:00	06:00	09:00	12:00	15:00	18:00	21:00	00:00
0600	06:00	09:00	12:00	15:00	18:00	21:00	00:00	03:00
0900	09:00	12:00	15:00	18:00	21:00	00:00	03:00	06:00
1200	12:00	15:00	18:00	21:00	00:00	03:00	06:00	09:00
1500	15:00	18:00	21:00	00:00	03:00	06:00	09:00	12:00
1800	18:00	21:00	00:00	03:00	06:00	09:00	12:00	15:00
2100	21:00	00:00	03:00	06:00	09:00	12:00	15:00	18:00

fraction (as determined from UCLEM) and the fractional weighting of the up to five vegetation classes within that grid cell. For the non-urban run (NV), which has no urban fraction, the grid cell values come only from the vegetation. This differencing method contrasts with the method typically used to determine urban effects, which computes the difference between an urban grid point and a nearby non-urban grid point (e.g., Hertwig *et al.*, 2021; Langendijk *et al.*, 2019). This is usually accomplished for individual cities, not for large or global areas, as our method allows.

2.4 | Determination of areal composites

To determine the impacts of urban areas on their surroundings, areal composites were computed for surface air temperature and precipitation centered on grid cells with greater than 10% urban fraction for regions of 5° north–south $\times 5^{\circ}$ east–west extent for every three hours of LTP. Grid cells with smaller than 10% urban fraction were considered to have no significant influence and were ignored based upon the results of Katzfey *et al.* (2020). Means were then computed from the data for all the selected regions for each season and for urban areas north of 23° N (NET, 274 urban cells), south of 23° S (SET, 39 urban cells) and the rest of the world (Tropics, 26 urban cells). The composites of urban fraction, as well as other selected surface fields for each latitudinal band, can be seen in Supplementary Figure S1.

Note that:

1. Some urban areas cover multiple grid cells, although each grid cell is treated separately when computing composites. Therefore, the larger urban areas will contribute to the area surrounding the central grid cell resulting in the composite mean being non-zero for neighboring grid cells (i.e., regional effects are partly due to neighboring urban grid cells). Composite figures include dotted lines where composite mean urban fraction is 5%, 10% and 15%.
2. No special treatment was made to handle land, water and surface height in the computation of composites; they are ignored.
3. There is no weighting for urban fraction – all grid cells with greater than 10% urban fraction are treated equally. Testing with and without weighting showed little difference.

2.5 | Determination of statistical significance

The statistical significance of the difference between the NVNU (with urban) simulation and the NV (non-urban)

simulation was calculated with the two-sided *t*-test using daily three-hourly LTP data from each simulation for the selected latitudinal band and grid cell with urban fraction greater than 10%. The Python scipy *t*-test² was applied for each urban grid cell and LTP and then averaged over all grid cells within a given LTP, season and latitudinal band. Note that this is different from the method in Katzfey *et al.* (2020) where the *t*-test was applied to annual mean values.

3 | DIURNAL CYCLE GLOBALLY

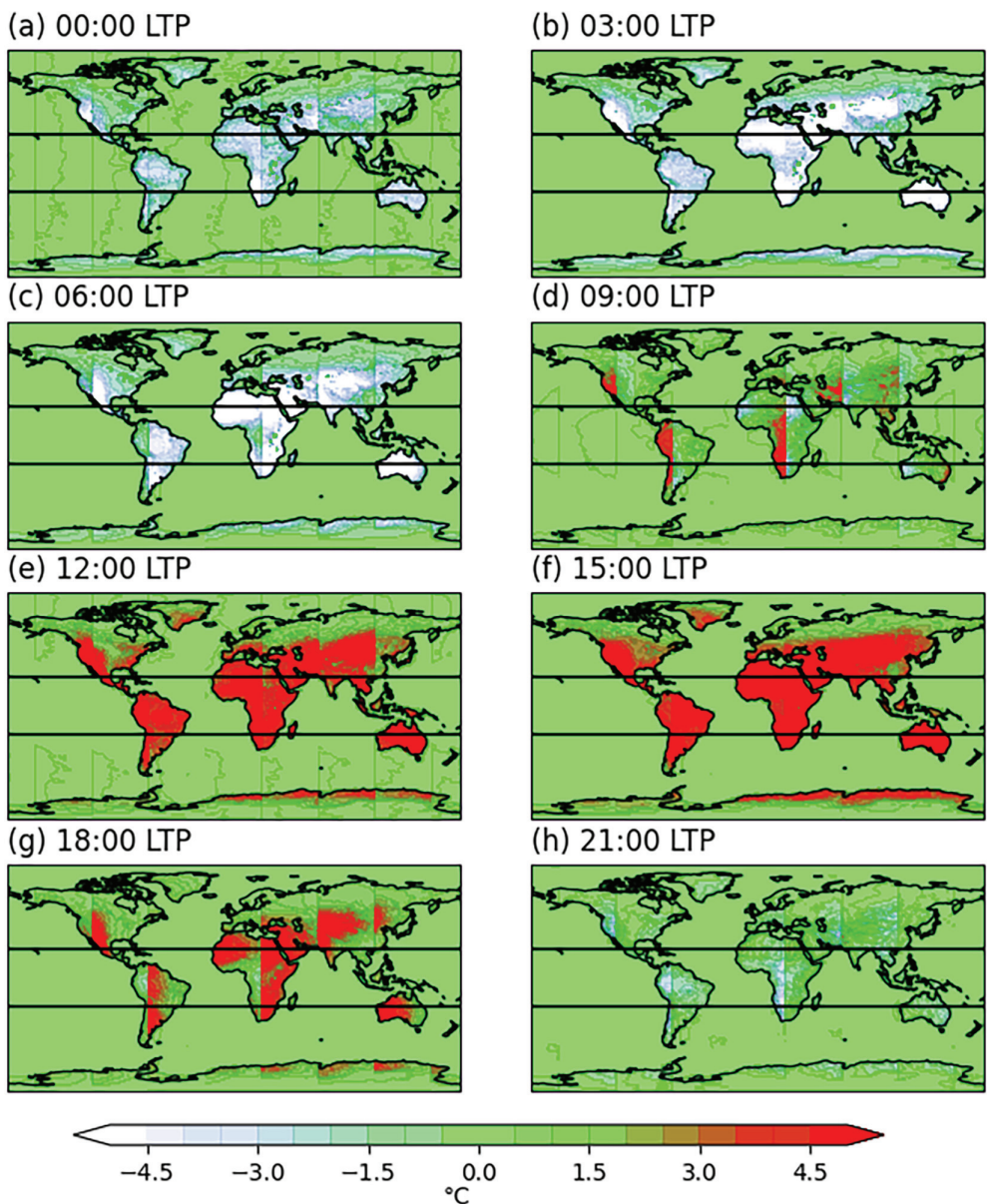
3.1 | Temperature

As has been documented before, the primary impact of urban areas is on the daily minimum air temperature (e.g., Katzfey *et al.*, 2020; Oke *et al.*, 2017; WMO, 2023). As the focus of this paper is on the diurnal cycle, the first step is to assess the diurnal cycle of temperature globally. The differences of annual mean Tasmax and Tasmin from the annual mean temperature (Figure 1) show the smallest diurnal signal in polar regions and oceans (as low as 2°C) and the largest signal in the subtropics (more than 10°C). The differences in magnitude of the diurnal signal show that for urban areas located in different latitudinal bands, the same intensity of the UIT potentially may have different relevance for the local and regional climate.

By calculating the mean temperatures every three hours LTP (Section 2.3), one can similarly assess the deviations of the temperature around the globe at similar local times. The differences of the annual mean temperatures at every three hours LTP from the annual mean temperature are shown in Figure 2. As expected, the lowest temperatures are at 00:00, 03:00 and 06:00 LTP (Figure 2a–c), while the highest temperatures are at 12:00, 15:00 and 18:00 LTP (Figure 2e–g), with intermediate temperatures at other times.

The LTP analysis method (Section 2.2) results in sharp differences between adjacent longitudinal bands and gradients within one LTP for some times. These are most pronounced during the periods of large temperature increases or decreases in the morning and evening (06:00–09:00 and 18:00–21:00 LTP). They are related to the differences in local temperatures within the three hours each LTP covers resulting from different incoming radiation at the eastern and western edges of the 45° longitudinal LTPs. The temperature range of the differences might reach 4°C within one LTP at average local sunrise time (Figure 2d) or in the LTP after average local sunset time (Figure 2g). However, later at night and during the day the differences are smaller, being hardly noticeable at 03:00 and 15:00 LTP. The ranges found within one LTP have little influence

FIGURE 2 Annual mean differences in three-hourly surface air temperature (Tas) from daily mean ($^{\circ}\text{C}$). (a) 00:00 LTP, (b) 03:00 LTP, (c) 06:00 LTP, (d) 09:00 LTP, (e) 12:00 LTP, (f) 15:00 LTP, (g) 18:00 LTP, (h) 21:00 LTP. Values are computed by subtracting daily mean from three-hourly LTP values for the simulation including urban areas (NVNU).



on the assessment of local and regional urban influences, because they occur in both the urban and non-urban simulations.

3.2 | Precipitation

The climatological mean precipitation (Figure 3) shows a realistic distribution of precipitation in the model simulation (see observed rainfall distributions in Figures S2 and S3).

The diurnal cycle of simulated precipitation in NVNU can be determined by subtracting the daily mean rainfall rate from the three-hourly mean rainfall rate (Figure 4).

Rainfall peaks at around 15:00–18:00 LTP over land while the peak over the tropical ocean occurs at around 06:00–09:00 LTP, which corresponds well with observations (e.g., Minobe *et al.*, 2020). As seen for Tas, some differences between adjacent longitudinal bands are evident for Pr. They are most pronounced over the tropical and subtropical land areas for 12:00 LTP and 21:00 LTP (Figure 4e,h). This can be explained by the strong increase (decrease) in rainfall rates before (after) the peak in the afternoon and early evening hours. As this study is focused on the comparison of the simulation with urban areas with the simulation without urban areas (i.e., a sensitivity study), no further validation of the results is presented here.

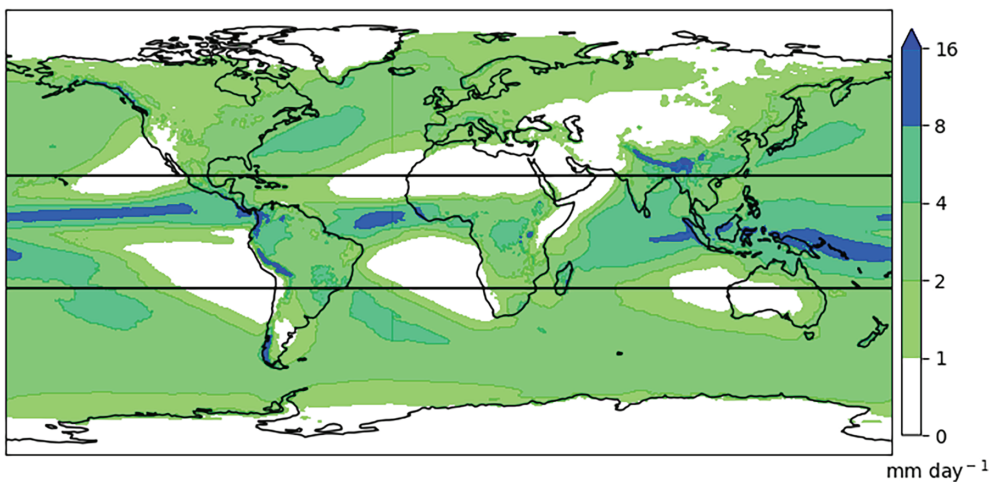


FIGURE 3 Annual mean precipitation (mm day^{-1}) for the period 1985–2010 from simulation including urban areas (NVNU).

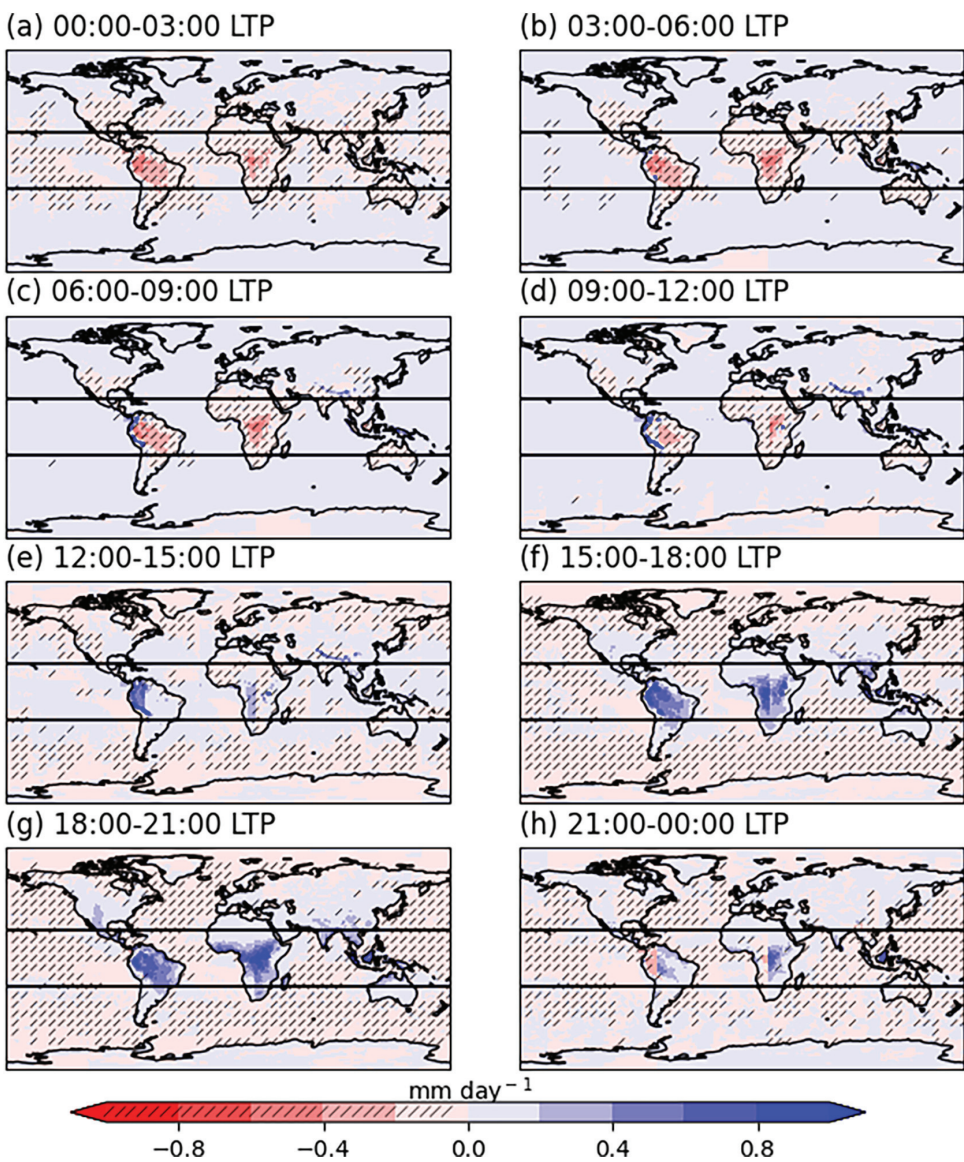


FIGURE 4 Three-hourly mean differences in surface precipitation from daily mean (mm day^{-1}). (a) 00:00–03:00 local time (LTP), (b) 03:00–06:00 LTP, (c) 06:00–09:00 LTP, (d) 09:00–12:00 LTP, (e) 12:00–15:00 LTP, (f) 15:00–18:00 LTP, (g) 18:00–21:00 LTP, h) 21:00–00:00 LTP. Values are computed by subtracting daily mean from three-hourly values. Negative values are hatched.

4 | IMPACT OF URBAN AREAS ON CURRENT CLIMATE

4.1 | Local urban influences

4.1.1 | Temperature

To assess the urban influences on the diurnal cycle of the temperature signal, 26-year mean temperature differences ($\text{NVNU} - \text{NV}$; Section 2.2) are calculated for each three-hourly LTP and each three-month season, and then related to the urban fraction. Figure 5 shows more warming during early evening and at nighttime (18:00, 21:00, 00:00, 03:00 LTP), with the largest values in JJA (Figure 5c; 21:00, 00:00 and 03:00 LTP). Maximum differences are below 1°C or even negative for 09:00 and 12:00 LTP in MAM (Figure 5b), JJA (Figure 5c), and SON (Figure 5d). This behavior is mainly caused by changes in the surface energy balance, with increases in sensible heat fluxes and heat storage and decreases in latent heat fluxes, due to the replacement of mainly vegetated land cover with urban land cover (i.e., buildings, streets etc.). Furthermore, anthropogenic heat fluxes are added to the energy balance, causing increases in near-surface temperature. These results confirm that urban areas have the greatest impact (warming) on the nighttime temperatures and there are greater effects for larger or more dense urban areas (WMO, 2023), visible in Figure 5 by the increases in temperature differences with increasing urban fraction. This effect is globally stronger in MAM and JJA and seems to be limited somewhat in DJF.

Considering that JJA and DJF are summer or winter depending on the hemisphere, these global results are partly averaging out summer/winter effects. Since urbanization is more intense in NET (274 urban grid cells in NET compared to 39 in SET), global average values for JJA (DJF) intensities are considerably influenced by results for NET summer (winter). This is illustrated in Figure 6, where JJA and DJF results for 00:00 LTP are compared for NET and SET. The UIT intensity is larger for the summer NET (Figure 6c) than for the summer SET (Figure 6b). Values are in general smaller for winter in both hemispheres, but winter NET values (Figure 6a) are still larger than winter values for SET (Figure 6d). Due to the larger and denser urban areas in NET, the winter values in NET are in fact of similar magnitude as the summer DJF values in SET. Note that the maximum UIT intensities are in the range of 3°C in NET, which in the northernmost parts of NET is above the diurnal temperature amplitude (Section 3.1).

To assess the local impact of urban areas for each LTP at various seasons and for different latitudinal bands of the

globe, composites were generated for urban grid cells (see Section 2.3). For each LTP and season, all grid cells with urban fractions greater than 10% were selected and resulting temperature values averaged. The results for Tas are shown in Figure 7 as Hovmöller-type diagrams (LTP on the ordinate and seasons on the abscissa).

Mean Tas composites for NVNU (upper left panels of Figure 7a–c) show that the temperatures are highest during the summer months in the extratropics (JJA in NET and DJF in SET) and lowest in wintertime (DJF in NET and Tropics and JJA in SET), as expected. In Tropics, there is little seasonal variation in Tas, but there are slightly larger values in MAM. The highest daily temperatures are generally from 12:00 to 18:00 LTP, most noticeably in the summer months of NET and SET, reflecting the diurnal cycle of the global temperature pattern (Figure 2).

The daily variability of the local temperatures as measured by the standard deviation in NVNU (upper right panels of Figure 7a–c) shows greater variability of the local temperatures (over 5°C) for NET spring (MAM) and autumn (SON). Similar but smaller variability also exists in SET. The smaller SET variability could be related to fewer inland cities. Little seasonal variation in Tas exists in the Tropics. All latitudinal bands have greater variability of Tas between 12:00 and 18:00 LTP.

The impact of urban areas on the local temperature is indicated by $\text{NVNU} - \text{NV}$ (upper middle left panels of Figure 7a–c). This shows warming at nighttime (00:00–06:00 and 18:00–21:00 LTP) for all latitudinal bands, with area average values up to 1°C for 00:00 and 21:00 LTP for NET in summer (JJA) and SET in spring (SON). There is little impact of urban areas at midday (09:00–15:00 LTP) for most seasons and latitudinal bands and even some small cooling effects occur (0 to -0.2°C at 09:00–12:00 LTP for NET in JJA). In Tropics, this cooling occurs for nearly the whole year at 09:00–12:00 LTP, except only at 12:00 LTP in MAM. In SET, the effect is seen at 09:00–12:00 LTP in DJF, but only at 12:00 LTP in MAM and JJA.

The percentage of grid cells with statistically significant differences in $\text{NVNU} - \text{NV}$ is shown in the lower panels of Figure 7a–c. This indicates that the nighttime differences (00:00, 03:00, 06:00, 18:00, 21:00 LTP) are statistically significant at the 95th percentile for all latitudinal bands for more than 80% of the urban cells.

The standard deviation between the NVNU and NV (middle right plots in Figure 7a–c) shows only small differences between the two simulations for all three latitudinal bands, generally less than 10% of the standard deviation of the NVNU simulation (upper right plots). This indicates only small changes in variability between NVNU and NV. It also implies that the mean changes are relatively robust.

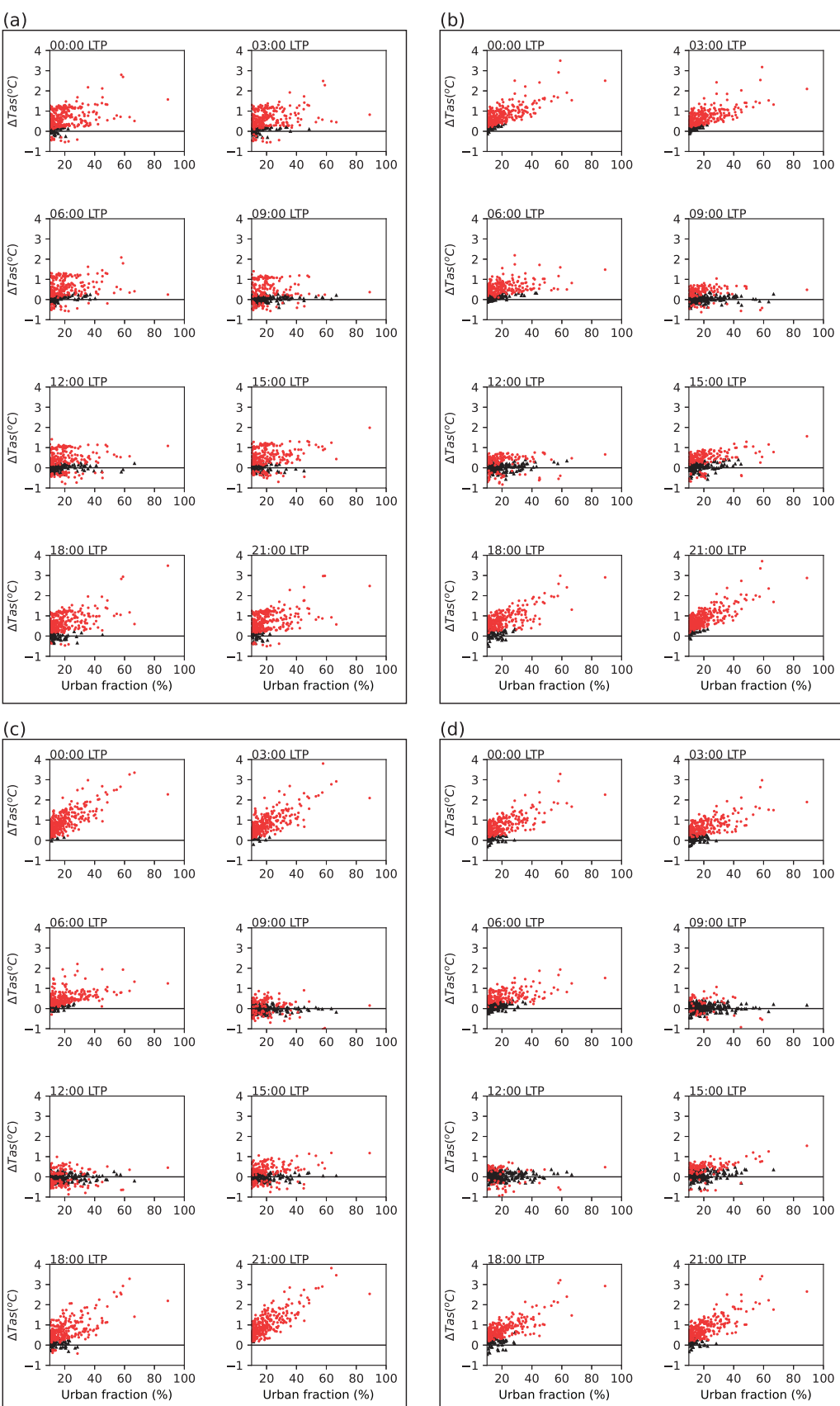


FIGURE 5 Plots of differences in surface air temperature (ΔT_{as} , $^{\circ}\text{C}$) for simulations with urban minus without urban areas (NVNU-NV) versus urban fraction (10%–100%) globally for all three-hourly local times (LTP) and seasons. (a) DJF, (b) MAM, (c) JJA, (d) SON. Each mark represents an urban grid cell. Red circles are statistically significant at the 95th percentile.

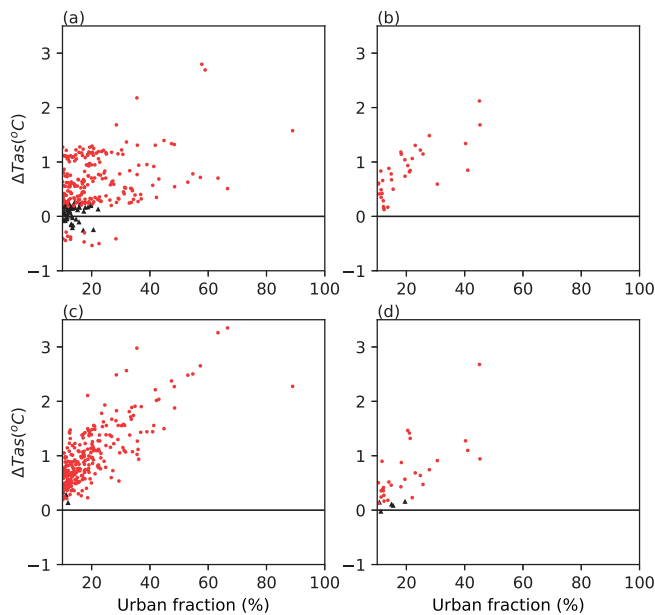


FIGURE 6 Plot of seasonal mean differences in surface air temperature (ΔTas , $^{\circ}\text{C}$) for simulations with urban minus without urban areas (NVNU – NV) vs urban fraction (10%–100%) for 00:00 local time (LTP). (a,b) DJF, (c,d) JJA. Northern extratropics (NET; 23° N to 90° N) on left (a,c) and southern extratropics (SET; 23° S to 90° S) on right (b,d). Each mark represents an urban grid cell. Red circles are statistically significant at the 95th percentile.

4.1.2 | Precipitation

In this section, the impact of urban areas on local precipitation is presented using the same methodology as for Tas presented above. As noted in Section 2 *Methodology*, values at given LTP are the accumulated precipitation for the three hours ending at that time. In the text following, the LTPs given are for the start to end of the accumulation period (i.e., 06:00 to 12:00 LTP means rainfall accumulated from 06:00 LTP to 12:00 LTP).

Relating the urban fraction to the LTP three-hourly accumulated precipitation globally (Figure 8) indicates that the local urban effect on rainfall tends to be small, but with some indication of consistent enhancement for some cities for 21:00 to 09:00 LTP (more than 60% of cities with positive change) coinciding with the positive temperature signal (Section 4.1.1). While few points are statistically significant (less than 15%, see Figure 8), those that are positive show increases for these LTPs as well (more than 75% of cities). Only for three-hourly precipitation ending at 18:00 LTP are more cities showing decreases than increases, both for all cities (54%) as well as for statistically significant cities (64%). These results suggest that some urban areas increase the nighttime precipitation and decrease precipitation for the three-hour period ending at 18:00 LTP. Note that these global results are dominated by

the larger number of NET urban grid cells than for Tropics or SET.

A method similar to that for temperature was used to determine the local impact of urban areas on precipitation for the different latitudinal bands. Averages were generated for grid cells with urban fraction greater than 10% (see Section 2.3) for each LTP and season. The results for Pr are shown in Figure 9 as Hovmöller-type diagrams (seasons on the abscissa and LTP on the ordinate).

The composite mean Pr for NVNU (upper left panels of Figure 9a–c) shows that the precipitation is generally similar in DJF, MAM and SON for all LTPs in NET except for the three hours ending at 09:00 LTP in MAM, where there is slightly more precipitation. During northern summer (JJA), the diurnal signal in rainfall is evident, with more precipitation in late afternoon (from 12:00 to 21:00 LTP) and less at night and in the morning (from 21:00 to 09:00 LTP). For the Tropics, there is more precipitation in the afternoon and evening (from 12:00 to 21:00 LTP) and less in the night and morning (from 21:00 to 09:00 LTP) for all seasons. In SET, the most precipitation is in DJF (summer) with more from 09:00 to 21:00 LTP. The season with the least precipitation is JJA (winter), which also shows little diurnal signal.

To verify the results for the diurnal precipitation cycle found in this study, Supplemental Figure S4 compares the NVNU simulation with ERA5 reanalysis data. The NVNU simulations capture the timing of the afternoon peak in precipitation in the Tropics and during summer in NET and SET. While the afternoon precipitation peak is less than in ERA5, the ERA5 reanalysis is on a 0.25° grid, while our simulations are on a 0.5° grid. In addition, Watters *et al.* (2021) indicated that the ERA5 reanalysis data tended to have a later afternoon peak than observed. A more thorough validation of the simulations is beyond the scope of this study.

The daily variability of the local three-hourly precipitation, as measured by the standard deviation in NVNU (upper right panels of Figure 9a–c), shows a mixed pattern for seasons and LTPs for all latitudinal bands. Only small variations in variability are noted for NET and Tropics. However, for SET, there is more variability in DJF and SON, especially from 06:00 to 21:00 LTP in DJF, and less variability in JJA. Apart from DJF, the other seasons have little variation of variability throughout the day.

The mean impact of urban areas on the local three-hourly precipitation over all cities in each region is indicated by the difference NVNU – NV (middle left panels of Figure 9a–c). Generally, the urban impact on the mean three-hourly precipitation for the corresponding LTP is less than 10% of the mean precipitation. The average change for all grid cells in NET shows generally small increases for most LTPs and seasons, except from 09:00

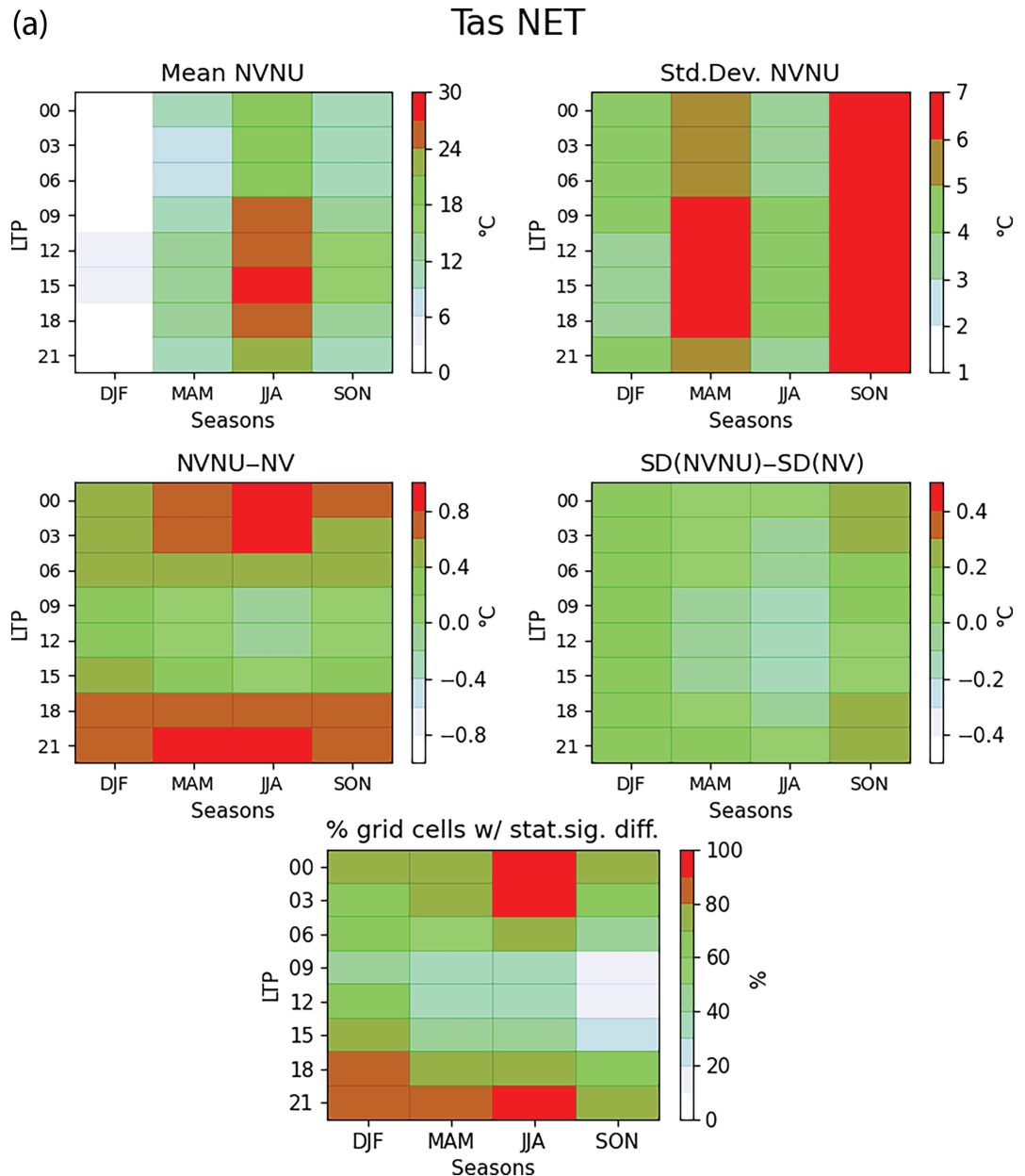
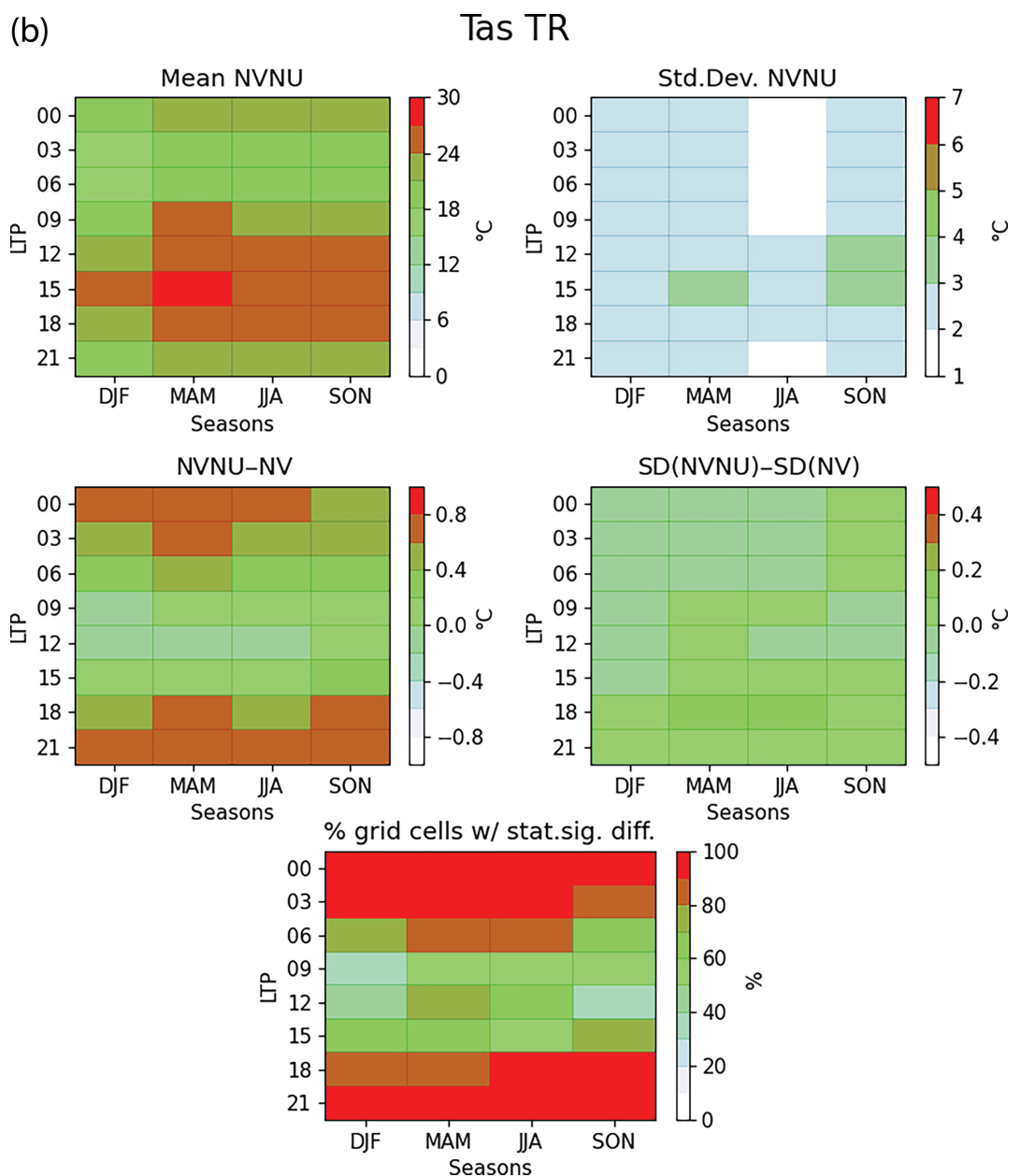
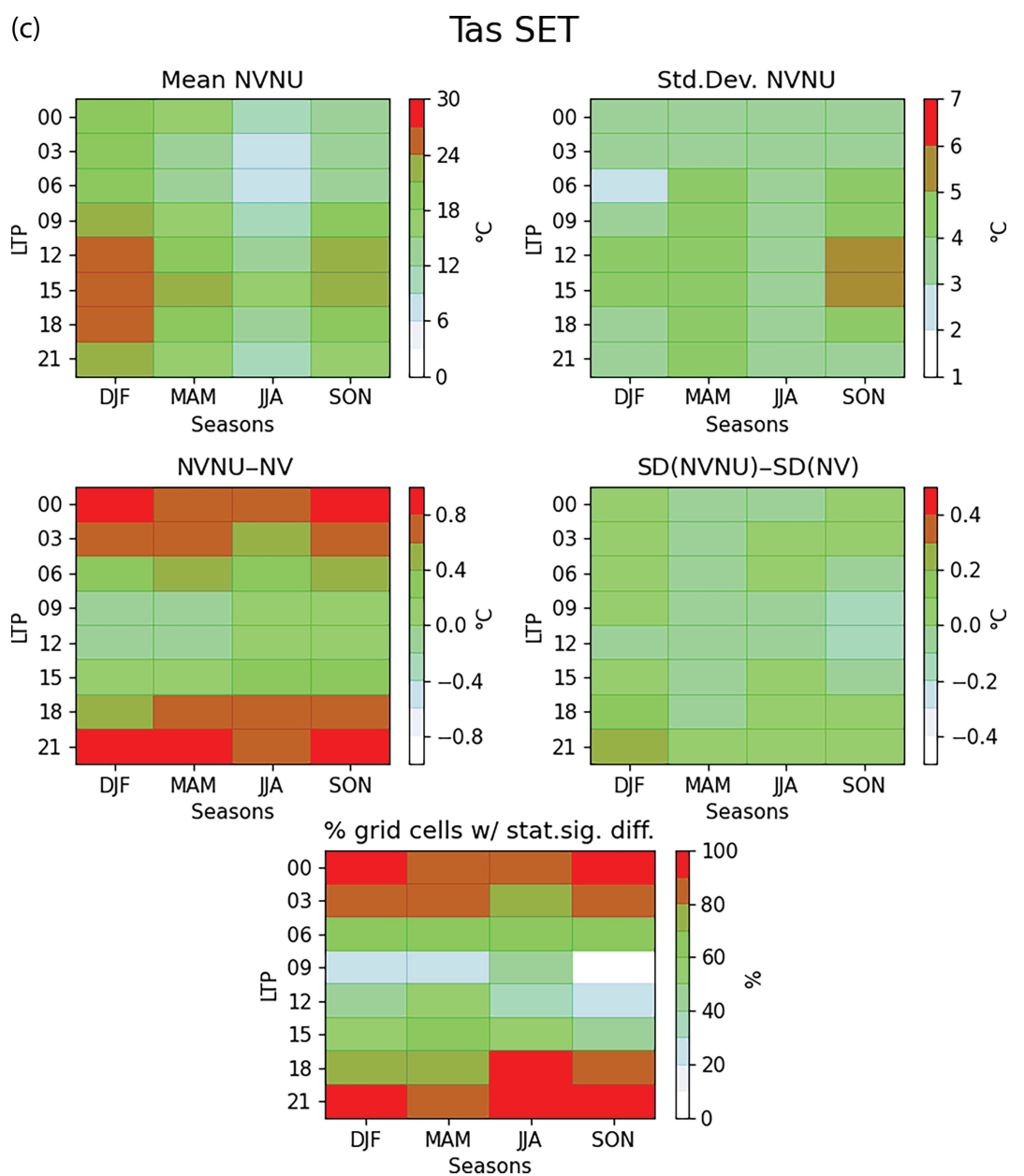


FIGURE 7 Season vs local time (LTP) of Tas composites for urban areas greater than 10% grid cell fraction: (a) northern extratropics (NET; 90° N to 23° N), (b) Tropics (23° N to 23° S) and (c) southern extratropics (SET; 23° S to 90° S). The upper left panel in (a–c) shows means for simulation including urban areas (Mean NVNU, °C), the middle left panel shows the urban effects (mean difference between simulations including and excluding urban areas [NVNU – NV], °C), the bottom panel is the percentage of grid cells with statistically significant differences at the 95th percentile (% grid cells w/ stat. sign. diff.), the upper right panel gives the standard deviation over time of NVNU (Std. Dev. NVNU, °C) and the middle right panel gives the difference in standard deviation NVNU – NV (SD_NVNU – SD_NV, °C).

**FIGURE 7** (Continued)

**FIGURE 7** (Continued)

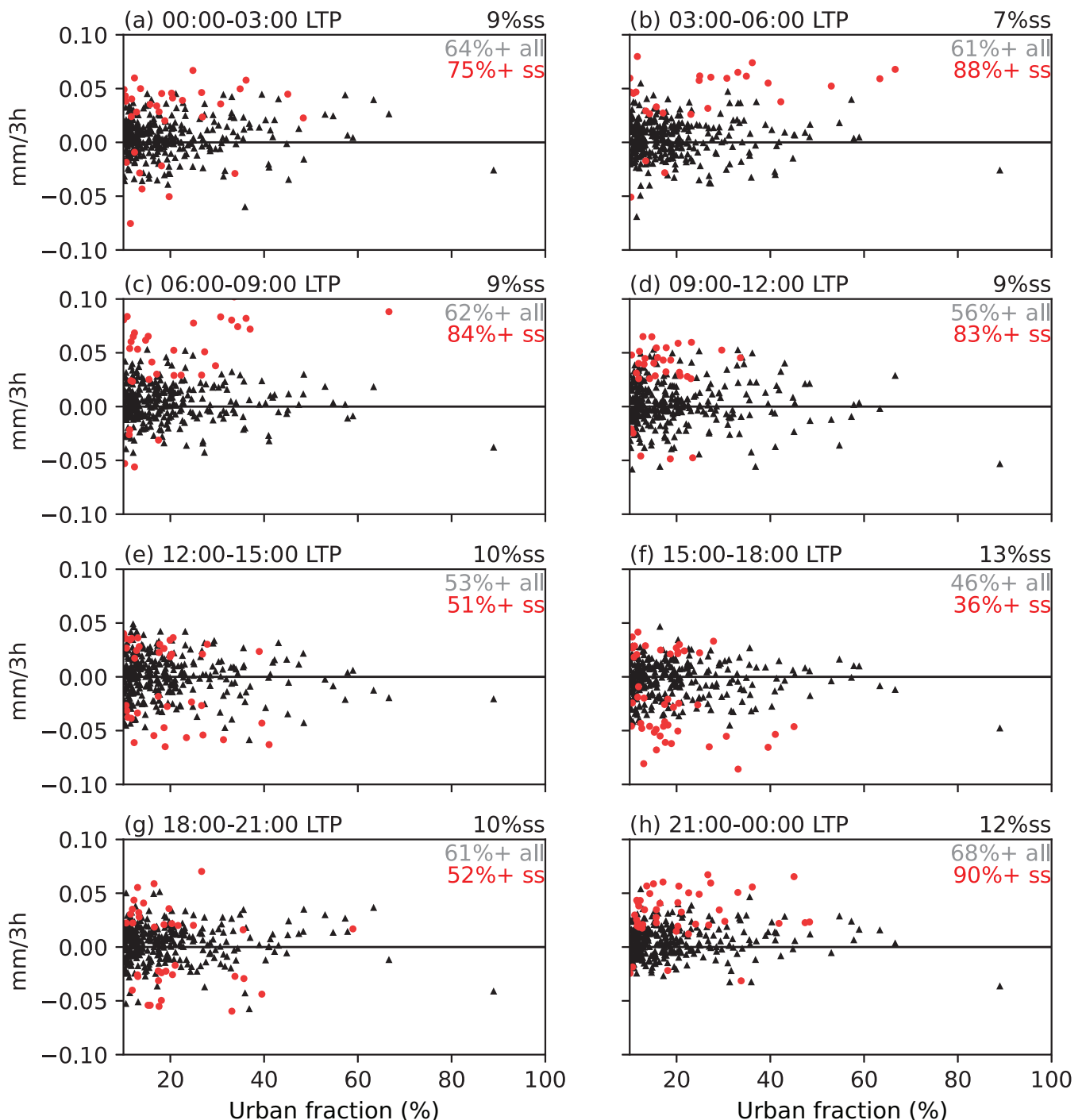


FIGURE 8 Annual differences in surface three-hourly accumulated precipitation (Pr , mm) vs urban fraction (%) (a) 00:00–03:00 local time (LTP), (b) 03:00–06:00 LTP, (c) 06:00–09:00 LTP, (d) 09:00–12:00 LTP, (e) 12:00–15:00 LTP, (f) 15:00–18:00 LTP, (g) 18:00–21:00 LTP, (h) 21:00–00:00 LTP. Values are computed by subtracting NV (which excludes urban areas) from NVNU (which includes urban areas). Red circles are statistically significant at the 95th percentile. Black horizontal line marks zero. Percent statistically significant values is noted above right of each panel (%ss). Inside each panel, black text indicates percent positive changes for all grid cells (+ all), while red text indicates percent of grid cells with statistically significant changes which are positive (+ ss).

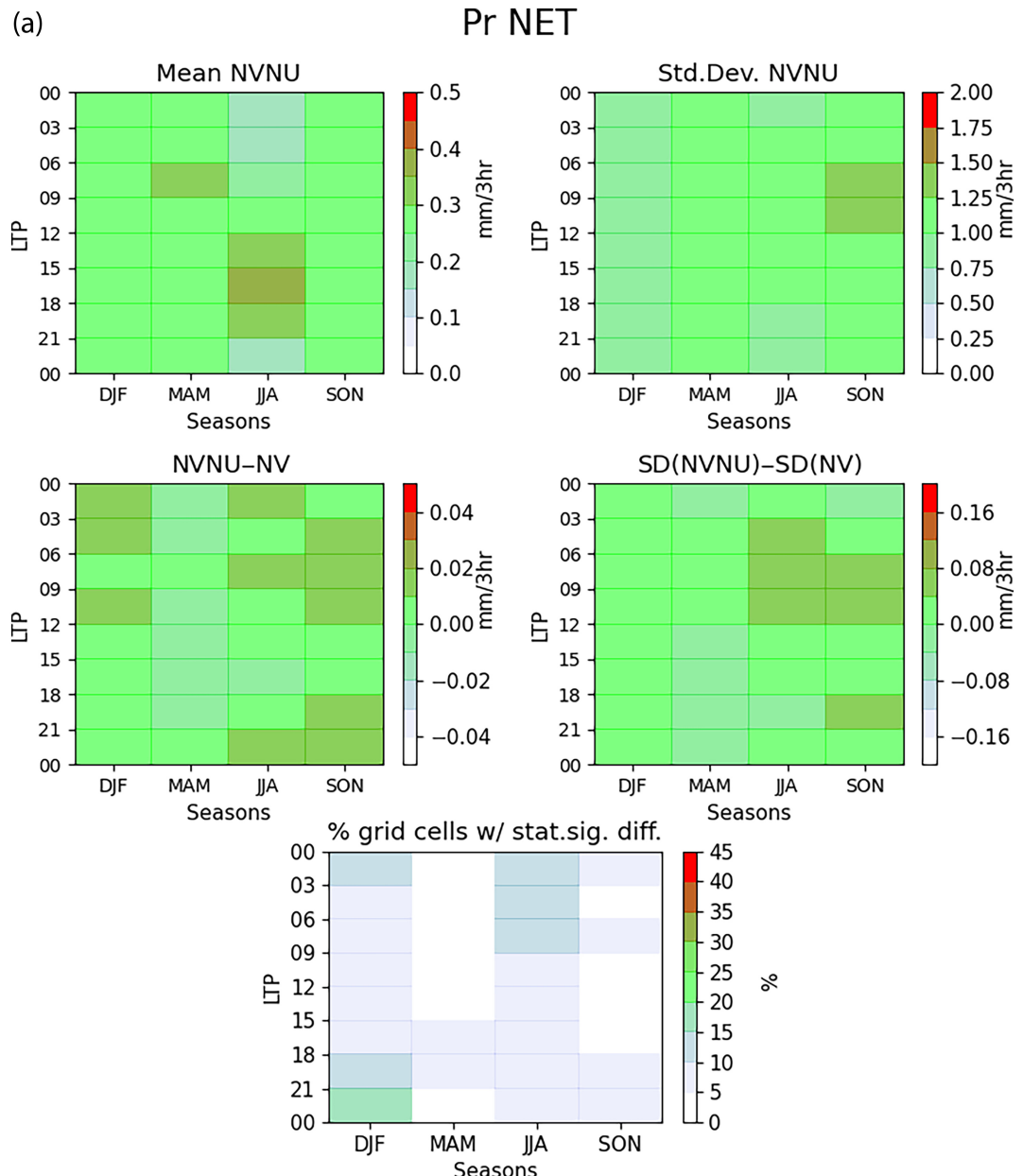
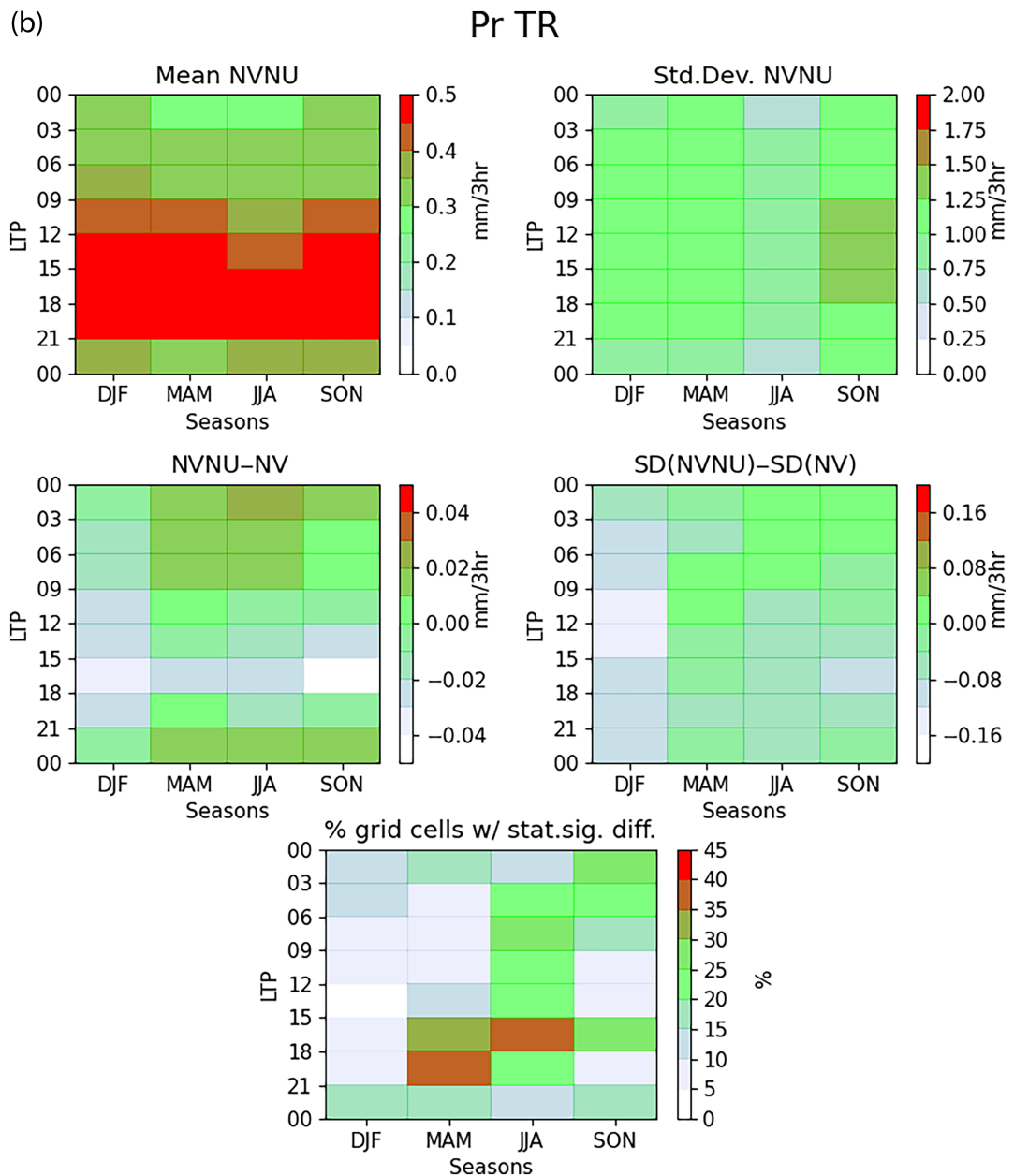


FIGURE 9 Season vs local time (LTP) of composites for three-hourly accumulated precipitation (Pr , mm) for urban areas greater than 10% grid cell fraction. (a) Northern extratropics (NET; 90°N to 23°N), (b) Tropics (23°N to 23°S) and (c) southern extratropics (SET; 23°S to 90°S). The upper left panel in (a–c) shows means for simulation including urban areas (Mean NVNU, mm accumulated per three hours), the middle left panel shows the urban effects (mean difference of simulations including and excluding urban areas [$\text{NVNU} - \text{NV}$], mm accumulated per three hours), the bottom panel is the percentage of grid cells with statistically significant differences at the 95th percentile (% grid cells w/ stat. sign. diff.), the upper right panel gives the standard deviation over time of NVNU (Std. Dev. NVNU, mm accumulated per three hours) and the middle right panel gives the difference in standard deviation NVNU – NV ($\text{SD}_{\text{NVNU}} - \text{SD}_{\text{NV}}$), mm accumulated per three hours).

**FIGURE 9** (Continued)

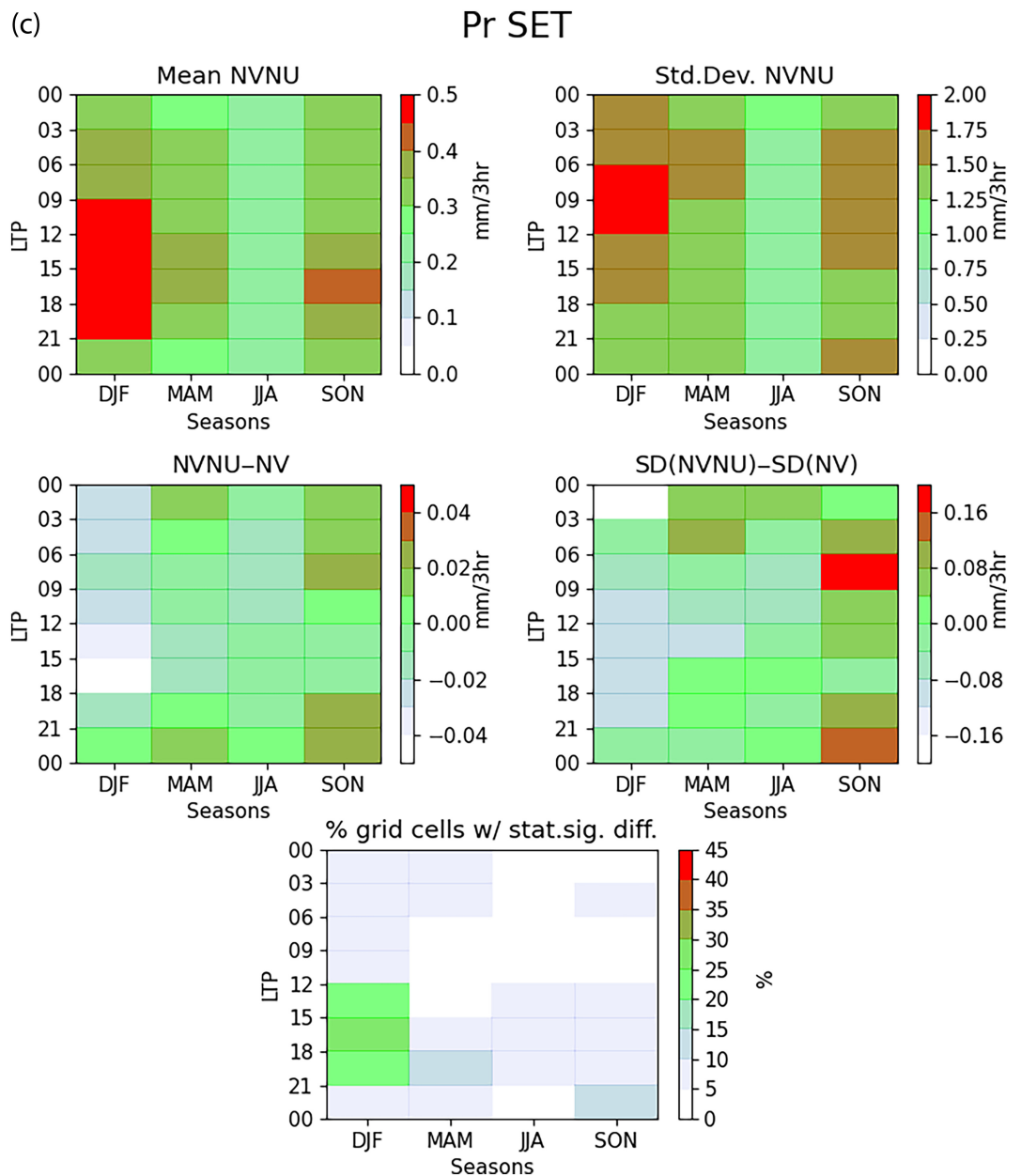
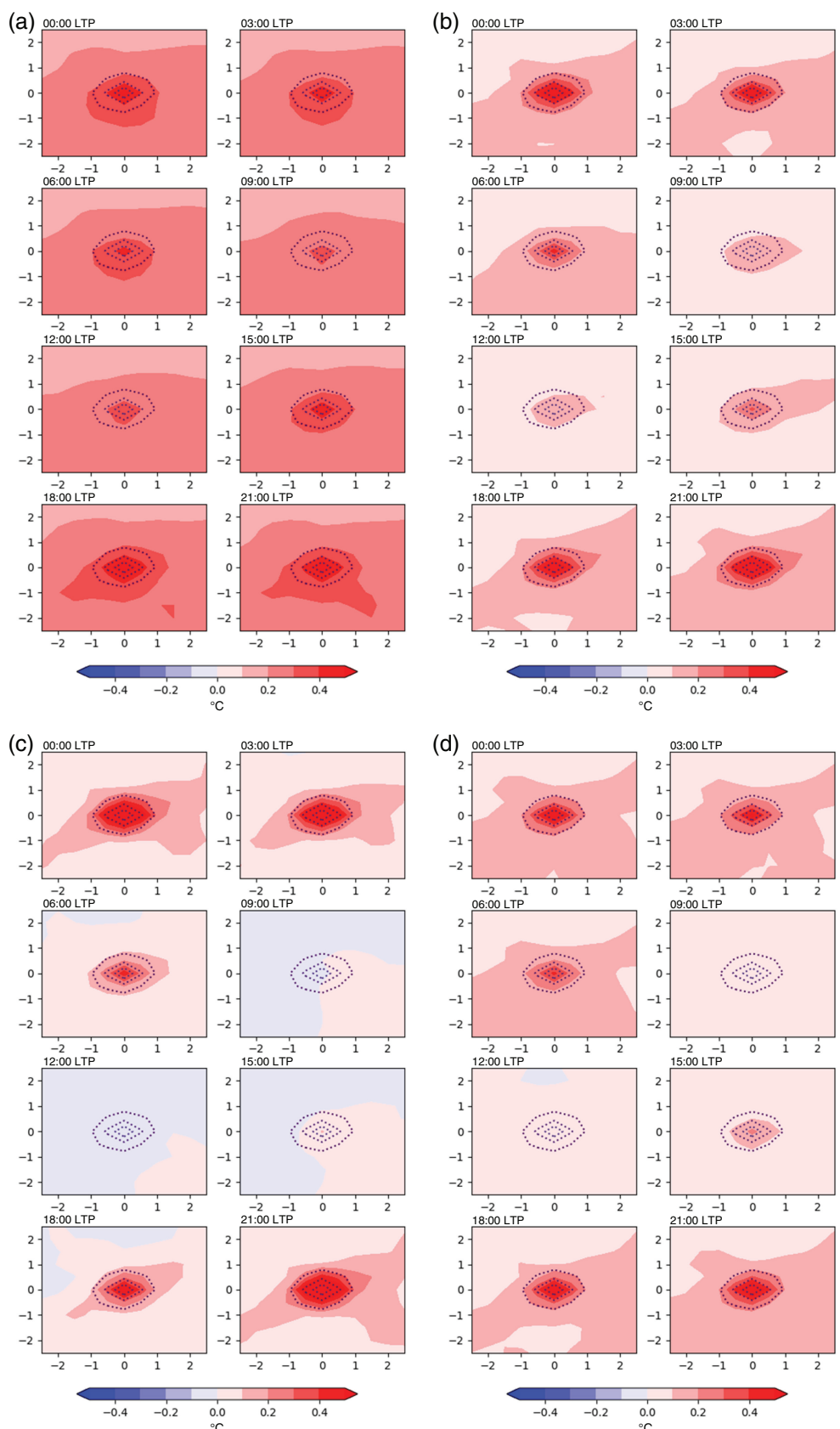


FIGURE 9 (Continued)

FIGURE 10 Composites of Tas ($^{\circ}C$) differences between simulations including and excluding urban areas (NVNU – NV) for urban areas in the northern extratropics (NET) for different seasons (a) DJF, (b) MAM, (c) JJA and (d) SON. In the subpanels, 00:00 local time (LTP) is on top left, 03:00 LTP on top right, following this pattern to 21:00 LTP on bottom right. Dotted lines are composite mean urban fraction at 5% (outer line), 10% (middle line), and 15% (innermost line). X- and y-axes are degrees from grid cell with urban fraction greater than 10%.



to 21:00 LTP and from 00:00 to 06:00 LTP for MAM and for 15:00 to 18:00 LTP in JJA. In the Tropics, increases in precipitation due to cities are indicated from 21:00 to 09:00 LTP for MAM, JJA and SON. Decreases are noted for all seasons for 15:00 to 18:00 LTP and for 12:00 to 15:00 LTP and 18:00 to 21:00 LTP except for MAM. Precipitation decreases are evident in SET for DJF for all LTPs except 21:00 to 00:00 LTP. All other seasons have decreases from 12:00 to 18:00 LTP and increases for 21:00 to 00:00 LTP. During SON, the increases extend from 18:00 to 12:00 LTP. For MAM, decreases are noted from 06:00 to 18:00 LTP and increases for the other LTPs. Finally, JJA shows mostly decreases in precipitation for all LTPs except from 21:00 to 00:00 LTP.

The percentage of cities with statistically significant differences in $\text{Pr}(\text{NVNU} - \text{NV})$, indicated by values greater than the 95th percentile using Student's t -test on daily data for each LTP, season and city) are shown in the lower panels of Figure 9a–c and are consistent with Figure 8. Overall, there is low significance of the differences for most cities (mainly less than 25%, with most less than 10%), while the percentage of statistically significant differences for Tas was above 80% for all urban area nighttime temperature increases. While there are slightly more LTPs and seasons with more statistically significant changes in the Tropics (up to 35%–40% significant increases for 18:00 to 21:00 LTP in MAM and for significant decreases from 15:00 to 18:00 LTP in JJA), the percentage of cities with significant differences is still small.

The standard deviation between the NVNU and NV (middle right plots in Figure 9a–c) shows small differences between the two simulations for all three latitudinal bands, generally less than 10% of the standard deviation (upper right plots), similar to Tas. Note that the magnitude of these changes is about four times larger than the changes in the mean, indicating larger uncertainty in the changes and making detection of mean urban effects on Pr difficult to determine. These results indicate that the differences in Pr due to urban effects are highly variable across all urban grid cells and much larger than for Tas. The urban impact on Tas is more consistent across the globe than for Pr .

4.2 | Regional urban influences

4.2.1 | Temperature

The regional impact of the urban areas can be assessed by creating composites for a 5° E–W by 5° N–S region centered on all grid cells with urban fraction greater than 10% and then examining the mean difference of NVNU – NV. As noted in Section 2.4, larger urban areas cover more than

one grid cell so that the composite means of urban fraction will be non-zero for neighboring grid cells in the composite (see dotted lines in Figure 10 of 5%, 10% and 15% mean urban fraction in the surrounding region in the composite). The mean Tas composite differences for urban areas in NET every three hours (Figure 10) clearly shows a warming in and around urban areas for 18:00–06:00 LTP in all seasons. In general, the warming is larger in the urban area than in the surroundings. For 09:00 to 15:00 LTP the values in the urban surroundings are small (MAM, SON) or around zero (JJA). In DJF local and regional warming is evident at all times and is likely caused by the high density of cities in NET, especially in Europe (as noted in Katzfey *et al.*, 2020). Note that the pattern of greatest warming is frequently orientated from SW to NE centered over the urban cell, most notable in JJA at night. As can be seen in Figure S1a, this pattern aligns with nearby urban areas contributing to the composite, most evident in the maximum urban fraction in the composite.

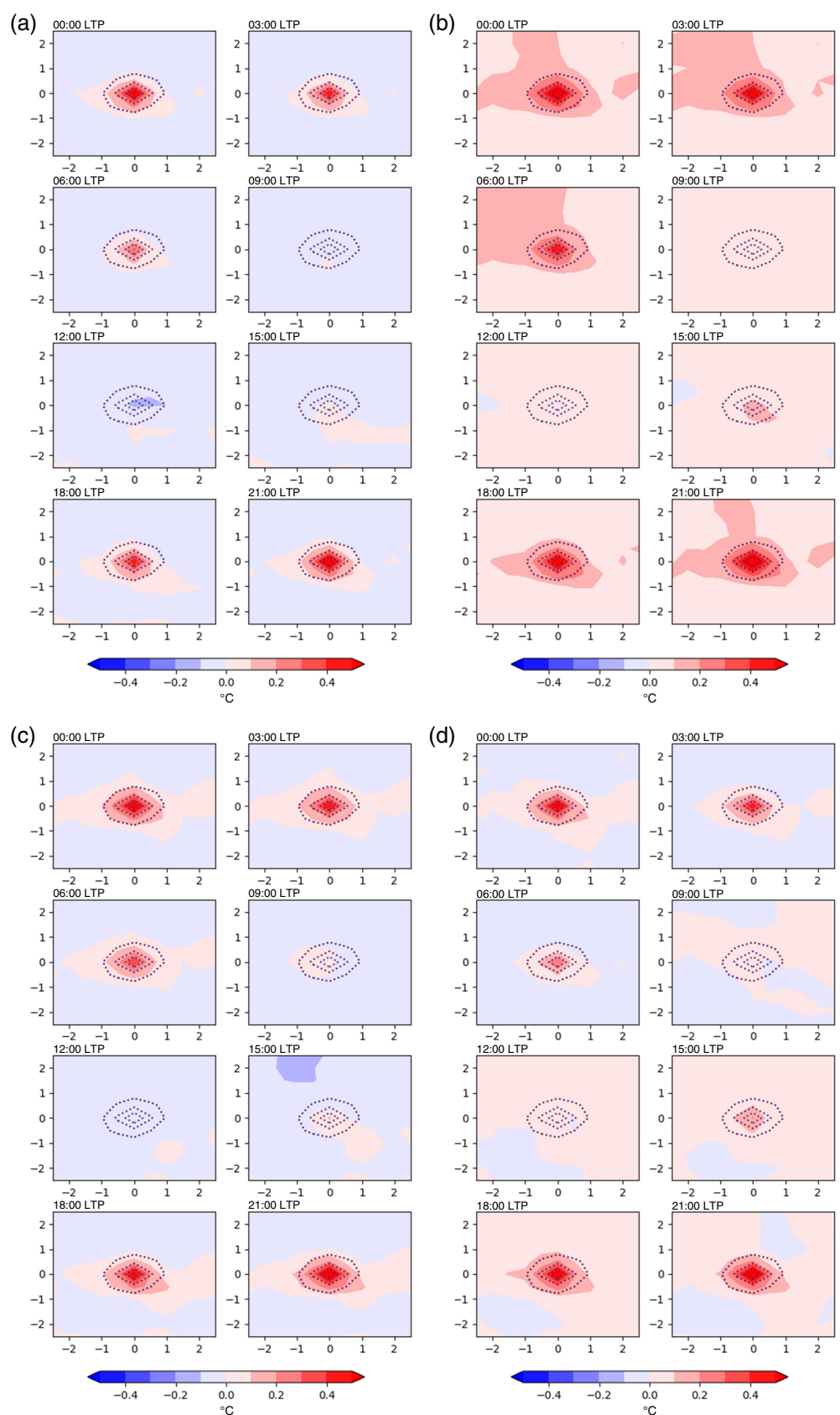
The regional composite of urban areas in the Tropics (Figure 11) shows local warming of more than 0.5°C over the urban grid cells at 18:00–03:00 LTP and a slightly lower value at 06:00 LTP. The regional impact is around zero with slight cooling (DJF, JJA, SON) or slight warming (MAM) for 06:00–15:00 LTPs. This small regional impact of urban areas can partly be explained by the urban fractions being nearly zero outside the urban cell (Figure S1b). In addition, the pattern of wind field differences (NVNU – NV) (see Figures S5–S7) shows a reduction of wind speed due to the rougher urban land cover likely leading to convergence and upward motion over the urban area for most seasons and times and which might also reduce the transport of the small UIT effect away from cities.

For SET (Figure 12), the impact of the urban areas on temperature is locally evident for all seasons from 18:00 to 06:00 LTP, reaching values of 0.5°C and higher at times. Regional warming due to urban areas is slightly noticeable for winter (JJA, especially for 15:00–21:00 LTP) and spring (SON, for 12:00–21:00 LTP). However, slight cooling in the greater surroundings is simulated for summer (DJF) for all times and in autumn (MAM) for 00:00–12:00 LTP north and northwest of the urban areas. While not pronounced, nearby cities are somewhat NW–SE (see Figure S1c).

4.2.2 | Precipitation

Similar to Tas, the regional impact of the urban areas on precipitation is assessed through analyzing the differences (NVNU – NV) of the mean composites for a 5° E–W by 5° N–S region centered on all grid cells with urban fraction greater than 10% (Section 2.4). Remember that the LTP

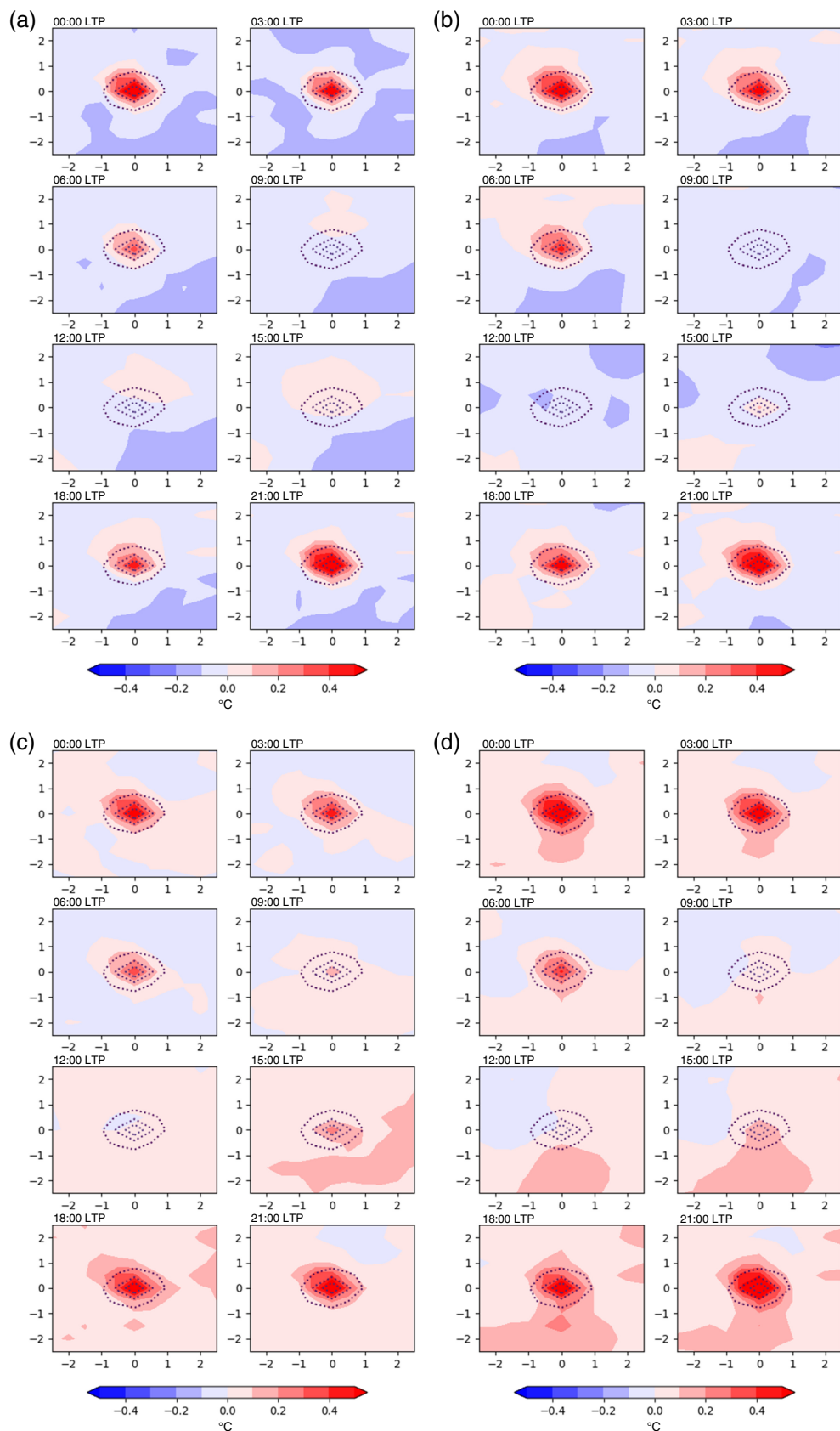
FIGURE 11 As Figure 10, but for Tropics.



ranges noted here are for the accumulation period for Pr. In general, the tendencies for increases/decreases found locally (Section 4.1.2) are also found in the surrounding

region in most cases. This can partly be explained by nearby urban areas contributing to the composite, at least for NET and SET (Figure S1).

FIGURE 12 As Figure 10, but for the southern extratropics (SET).

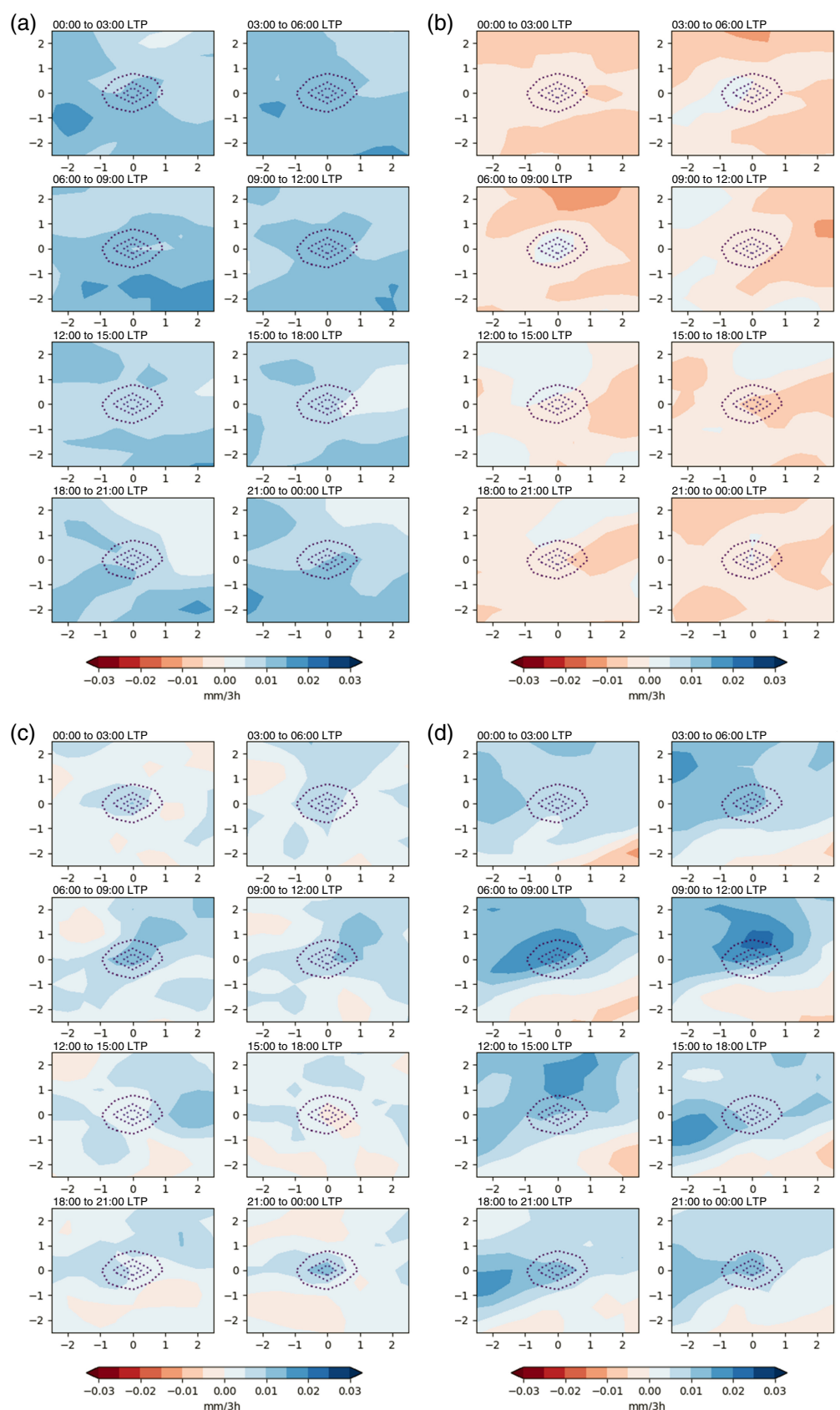


The differences of Pr for urban areas in NET for DJF every three hours (Figure 13a) show a general increase in Pr in urban areas and surrounding regions for all LTPs.

However, the increase in Pr seems to be slightly more to the south of the cities, a potential downwind effect (composite winds tend to be northerly; not shown), so the increases

FIGURE 13

Composites of three-hour accumulated precipitation (Pr , mm) differences of simulations including and excluding urban areas [$NVNU - NV$], in the northern extratropics (NET) ($23^\circ N$ to $90^\circ N$) for different seasons (a) DJF, (b) MAM, (c) JJA and (d) SON and different local times. Dotted lines are composite mean urban fraction at 5% (outer line), 10% (middle line), and 15% (innermost line). X- and y-axes are degrees from grid cell with urban fraction greater than 10%.



are not centered over urban areas. Some of this non-local pattern of differences might also be explained by the distribution of nearby cities (see Figure S1a). The pattern of the

number of cities within the composite and the maximum urban fraction within the composite shows that both have a SW-NE orientation of larger values through the center

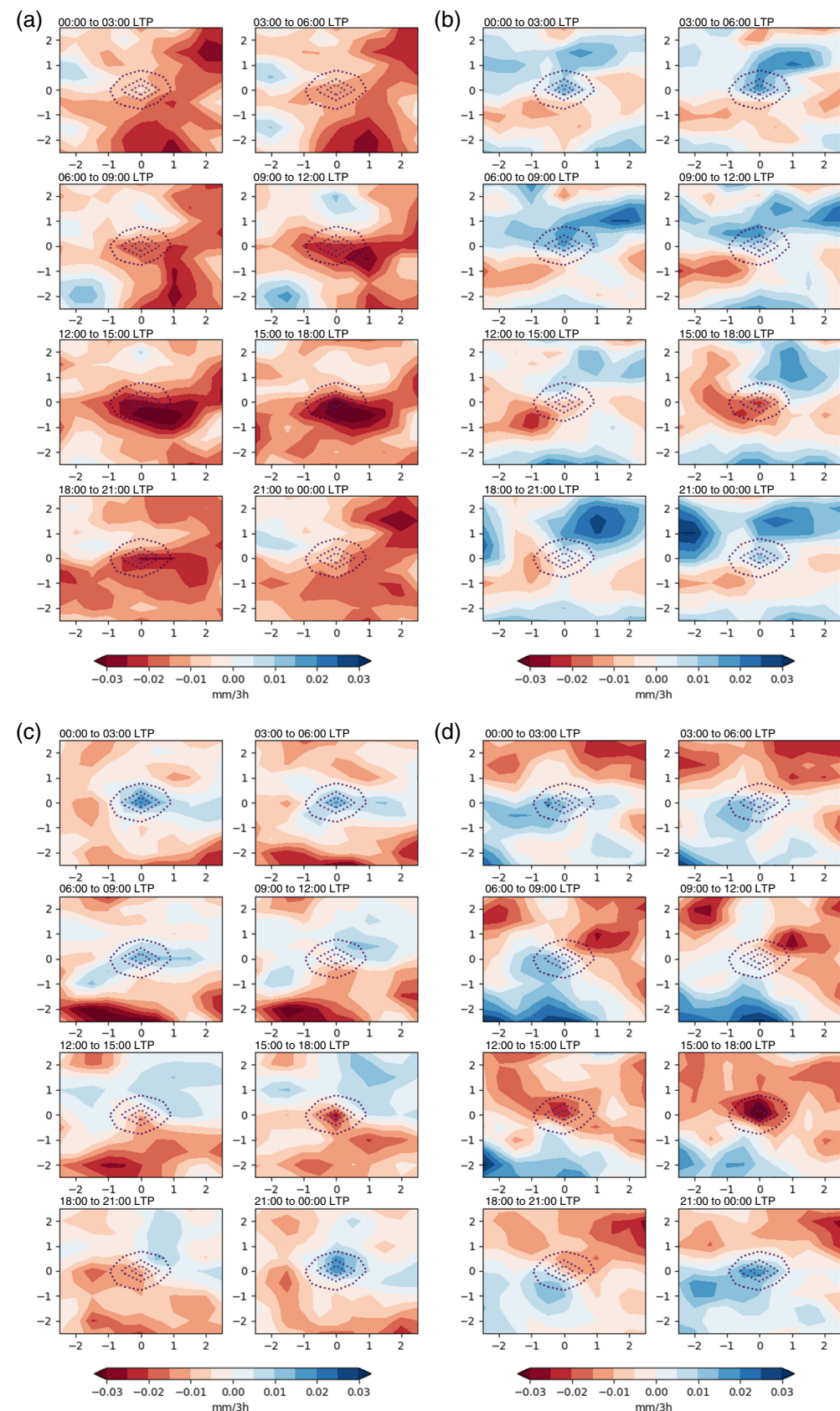
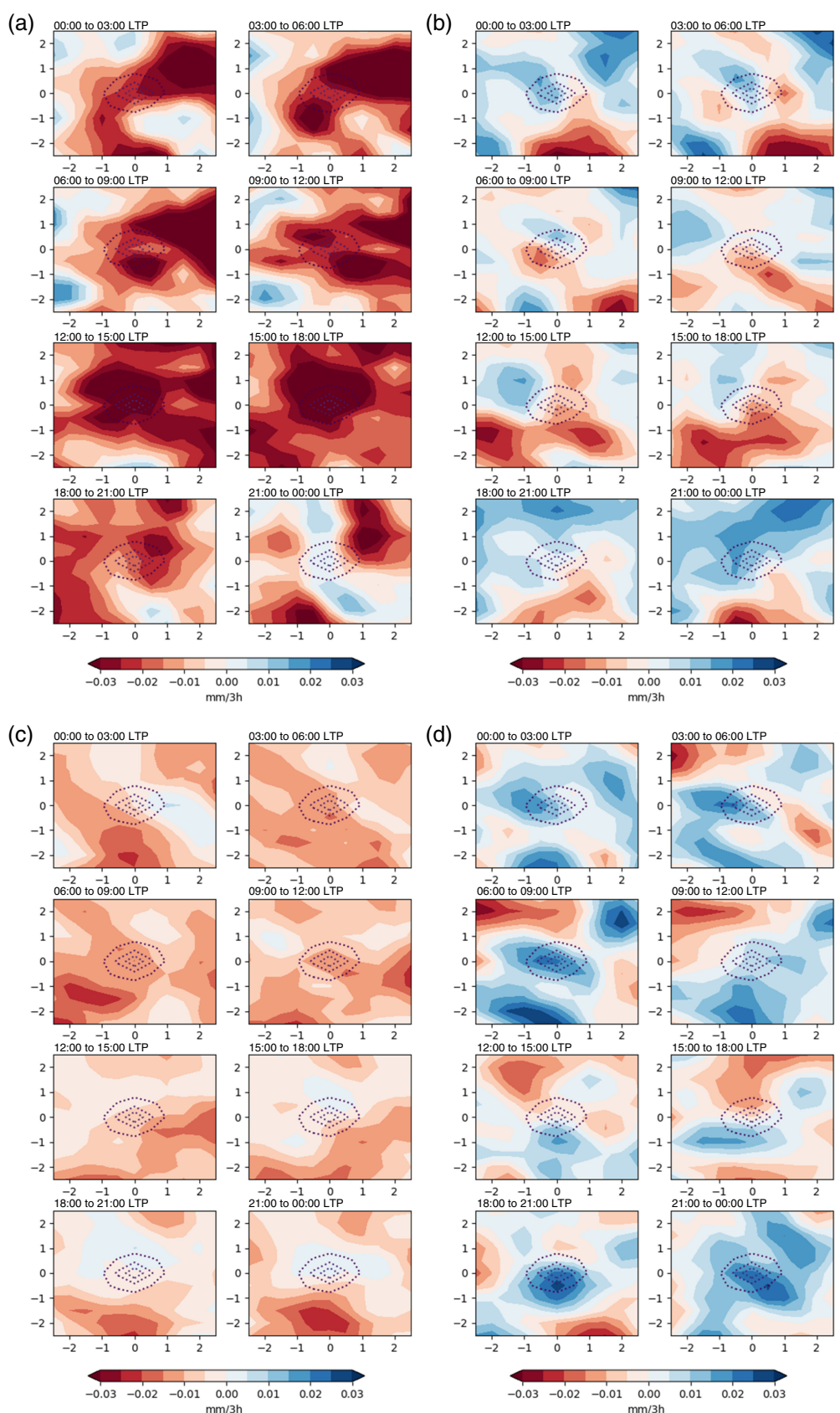


FIGURE 14 Same as Figure 13, but for Tropics.

of the composite, which could cause the similar pattern of increased rainfall for most LTPs. The pattern of changes for MAM (Figure 13b) shows general regional decreases

in precipitation. The decreases are slightly greater to the east, upwind of the cities. The cause for these changes is not clear. The regional increases in JJA (Figure 13c) are

FIGURE 15 Same as Figure 13, but for the southern extratropics (SET).



smaller than for DJF and SON but with some enhancement around cities, similar to DJF and SON, except for 15:00 to 18:00 LTP, where there are slight decreases. For

SON (Figure 13d), precipitation increases are noted in the composites with a general SW–NE orientation, again suggesting a potential influence of the surrounding urban

areas in the composite. The magnitude of the increases for SON is also somewhat larger than for the other seasons, consistent with local changes noted in Figure 9a.

In the Tropics, (Figure 14) the composite of regional changes in Pr indicates relatively large decreases surrounding the cities for DJF and JJA, while there is a combination of increases and decreases regionally for MAM and SON. Also note that the changes over the cities appear more localized, especially evident in JJA for the increases from 21:00 to 09:00 LTP and the decreases from 09:00 to 21:00 LTP. This might be due to fewer neighboring cities in the Tropics (see Figure S1b). The pattern of changes also tends to be slightly orientated W to E, which might be partly explained by the distribution of the maximum urban fractions and orography within the Tropics composite (see Figure S1b). Increases tend to be evident during early morning hours (from 21:00 to 09:00 LTP) and decreases during the late morning to evening (from 09:00 to 21:00 LTP) except for DJF. These results were also noted in Figure 9b.

For SET (Figure 15), regional decreases in Pr are evident for all LTPs except from 21:00 to 00:00 LTP in summer (DJF) and in winter (JJA). For the other transition seasons (MAM and SON), the pattern of differences is less clear, but with slightly more regional decreases for 12:00 to 18:00 LTP. For SON, the local increases for all times except from 12:00 to 18:00 LTP are also seen to some extent regionally. As noted in Figure 9c, there is an indication of increases for 00:00 to 03:00 LTP and of decreases for 15:00 to 18:00 LTP.

While detailed analysis of the causes of the rainfall changes is beyond the scope of this paper, preliminary results suggest possible mechanisms. Enhanced precipitation could be related to increases in Tas over urban areas leading to enhanced convection, as has been noted by previous studies (e.g., Han *et al.*, 2014; Liu & Niyogi, 2019). Enhanced convection and precipitation could also be triggered by the decreased wind speeds over urban areas (see Figures S5–S7) leading to convergence and enhanced upward motion over urban areas (not shown). Decreased rainfall could also be related to the reduced near-surface humidity (see composites of surface humidity in Figures S8–S10), caused by a reduced evapotranspiration in urban areas, leading to decreased convection. Finally, the decreased rainfall noted in early afternoon could be related to the slight cooling in Tas leading to reduced convection and rainfall. These mechanisms need further investigation.

5 | CONCLUSIONS

This study investigates the impact of urban areas on diurnal cycles of temperature and precipitation. A global model

(CCAM) was run at ca. 50 km resolution with and without an urban parameterization, and the differences between these two simulations are used to determine the impacts of urban areas. The method used to fill the urban areas with “appropriate” vegetation differs from those used in previous studies, where the determination of urban effects involves comparing station values within the city to a station outside the city. However, that method requires careful choice of stations.

One key aspect of this study was to globally aggregate the data in corresponding LTPs to assess the mean impact of urban areas on the diurnal cycle. A method to combine global data for grid cells with urban fractions greater than 10% for each local three-hour time period was then developed to more effectively analyze time-dependent differences of urban influences. By using these time zones, it was possible to assess periods of temperature changes, and to analyze the results for three latitude bands: 23° N to 90° N (NET), 23° S to 23° N (Tropics) and 23° S to 90° S (SET) for the four seasons. Results are presented for averages over all grid cells with urban fractions greater than 10%. Defining smaller zones/LTPs might help clarify the results, since at certain times of day there were large differences at the eastern and western edges of the zones, but these are consistently found in both simulations and thus have small influences on the urban signal. The influence of, for example, one-hour LTPs on results could not be tested, because available data were three-hourly. Therefore, only eight global zones were possible.

Results show the model was able to capture the urban impact on the diurnal temperature cycle, with the greatest urban influence on temperature (warming) from 18:00 to 03:00 LTP and a slight cooling effect at midday (12:00 to 15:00 LTP). This complements the findings of Katzfey *et al.* (2020) on the urban impact on Tasmin and Tasmax, which used the same dataset, by demonstrating the timing of the UIT. Note that the maximum UIT is around midnight, not at the time of temperature minimum. The pattern established for the urban effect on temperature throughout day and night matches well with other research (e.g., Oke *et al.*, 2017).

Results for urban impacts on precipitation were not as statistically significant as for temperature, which could partially be attributed to the large variability of rainfall. However, some interesting patterns were still noted. Overall, local and regional increases are most evident in the morning (00:00 to 12:00 LTP in NET, 00:00 to 09:00 in the Tropics and 00:00 to 06:00 LTP in SET, except for DJF and JJA). While the mean changes over all cities were relatively small, some urban grid cells did show larger urban impacts. Furthermore, the urban impacts on precipitation and temperature show broadly similar patterns, which would be unlikely if the changes were caused by internal

climate variability alone. Note that the results for SET and Tropics are possibly less robust because there are fewer urban grid cells relative to NET.

NET experienced enhanced local precipitation in all seasons except for 03:00 LTP and 12:00 to 21:00 LTP in MAM and 18:00 LTP in JJA. There were regional increases in precipitation except for MAM, when regional decreases were noted. The regional pattern of changes for NET suggests that precipitation was potentially influenced by the combined influences of nearby cities and prevailing winds.

The urban influence on regional precipitation in the Tropics was more mixed, with regional decreases more evident in DJF and JJA, despite the local increases between 00:00 and 09:00 LTP. For MAM and SON, the regional pattern of differences was more varied, with both increases and decreases in regional precipitation. Due to the urban effect of decreasing near-surface relative humidity and slight cooling, rainfall decreases were evident between 15:00 and 18:00 LTP for all seasons, possibly because convective precipitation was suppressed at these times. Further investigation is required for a more detailed understanding of the causes of these urban impacts.

This study suggested that the urban influence on precipitation in SET was for regional decreases for DJF and JJA and a more complicated pattern of increases and decreases in MAM and SON, similar to the Tropics. However, there was still a tendency for increases over the cities in early morning (00:00 to 06:00 LTP) in MAM and SON.

Increases (decreases) in urban precipitation that are frequently found for nighttime (midafternoon) suggest a possible influence of the urban heating (cooling) effect, respectively. Reduced surface moisture in urban areas could reduce convection and precipitation. Finally, increases in precipitation might be related to enhanced vertical motions related to lower wind speed over urban areas. These results are consistent with Liu and Niyogi's (2019) meta-analysis, which indicated that precipitation increases over the city and possibly in surroundings, with responses related to city characteristics and location. The slight early afternoon cooling could explain the decreased precipitation noted through decreased convection. Enhanced upward motion related to the lower wind speeds and larger boundary layer height over urban areas could also cause enhanced convection and precipitation. However, the generality of these results needs further investigation.

Results related to the research questions are:

1. The local impact of urban areas on Tas (warming) is evident during the night and is strongest in summer. Some slight cooling was noted around midday. The impact of urban areas on precipitation is small in the mean over many urban areas, with increases more

likely from 00:00 to 06:00 LTP and decreases from 15:00 to 18:00 LTP.

2. The regional impact of urban areas on the immediate surroundings is more evident at nighttime for temperature. While the regional urban impact for precipitation is more varied, some evidence suggests that nearby cities combine their urban effects to enhance the regional pattern. In the tropics, decreased afternoon rainfall might be related to changes in surface temperature and relative humidity over cities.

Katzfey *et al.* (2020) showed a global influence of urban areas on temperature. This study shows both local and regional impacts of urban areas on the diurnal cycles of temperature and precipitation, although the temperature signal is clearer than the precipitation signal. The magnitude and sign of the impact depend upon latitude band, season and time of day (LTP).

By analyzing simulations with different land surface covers, one with urban areas and one without, this study has helped to show that the results of GCMs employing urban parameterizations can be used to consider the impacts of urban areas on local and regional climate.

However, determining the causes of these responses is challenging because they are the result of an interplay of multiple processes, which also depend on the local meteorological and climatological conditions such as wind speed and boundary layer height, orography and surrounding vegetation, as well as the type of rainfall (convective vs stratiform), as studied by Shen and Yang (2023).

This paper presents the average effect of urban areas on local and regional temperature and rainfall using a single GCM employing a specific urban parameterization. Hence, a GCM intercomparison study would be desirable, like the WCRP Flagship Pilot Study URB-RCC (Langendijk *et al.*, 2024), where coordinated experiments will be carried out with convection-permitting regional climate models coupled with urban parameterizations of different complexity. Similarly, higher-resolution global model runs should be completed to increase the number of urban grid cells for more robust statistics, especially for the Tropics and SET. In order to further decrease the influence of the internal climate variability additional single-model experiments could be conducted, which could help to quantify the significance of the urban impact on precipitation. Furthermore, a more in-depth analysis of the causes of the rainfall changes should be done, setting up simulations for the purpose of determining the cause of rainfall increases at night. For such an analysis a further stratification of the results (e.g., by climate zone or inland vs coastal cities) or the analysis of individual cities is recommended. Changes in the urban impacts under climate change should also

be investigated, as well as the impact of urban areas on extremes.

ACKNOWLEDGEMENTS

The authors would like to thank Marcus Thatcher for the support given.

FUNDING INFORMATION

The work was supported through the Deutsche Forschungsgemeinschaft (DFG, German Research Foundation) within the Cluster of Excellence “CliSAP” (EXC177) and under Germany’s Excellence Strategy – EXC 2037 “Climate, Climatic Change, and Society - CLICCS” – Project Number: 390683824. Some work was conducted within the project LANDMATE funded by the Helmholtz Institute for Climate Service Science (HICSS), a cooperation between Climate Service Center Germany (GERICS) and Universität Hamburg. Part of the work was conducted within the CoSynHealth project, funded by the German Federal Ministry of Education and Research (BMBF) (01LN2204A) with the provision of management support from the German Aerospace Center (DLR).

DATA AVAILABILITY STATEMENT

Data are available upon request from the first author.

NOTES

¹ MODIS: These data are distributed by the Land Processes Distributed Active Archive Center (LP DAAC), located at the U.S. Geological Survey (USGS) Earth Resources Observation and Science (EROS) Center (lpdaac.usgs.gov), distributed in netCDF format by the Integrated Climate Data Center (ICDC, <http://icdc.cen.uni-hamburg.de>), University of Hamburg, Hamburg, Germany.

² https://docs.scipy.org/doc/scipy/reference/generated/scipy.stats.ttest_ind.html.

ORCID

Jack Katzfey  <https://orcid.org/0000-0002-0604-8860>

REFERENCES

- Bohnenstengel, S.I., Hamilton, I., Davies, M. & Belcher, S.E. (2014) Impact of anthropogenic heat emissions on London’s temperatures. *Quarterly Journal of the Royal Meteorological Society*, 140, 687–698. Available from: <https://doi.org/10.1002/qj.2144>
- Chapman, S., Thatcher, M., Salazar, A., Watson, J.E. & McAlpine, C.A. (2018) The effect of urban density and vegetation cover on the heat Island of a subtropical city. *Journal of Applied Meteorology and Climatology*, 57, 2531–2550. Available from: <https://doi.org/10.1175/JAMC-D-17-0316.1>
- Chen, L. & Frauenfeld, O.W. (2016) Impacts of urbanization on future climate in China. *Climate Dynamics*, 47, 345–357.
- Daniel, M., Lemonsu, A., Déqué, M., Somot, S., Alias, A. & Masson, V. (2019) Benefits of explicit urban parameterization in regional climate modeling to study climate and city interactions. *Climate Dynamics*, 52, 2745–2764. Available from: <https://doi.org/10.1007/s00382-018-4289-x>
- Di Virgilio, G., Evans, J.P., Di Luca, A., Olson, R., Argüeso, D., Kala, J. et al. (2019) Evaluating reanalysis-driven CORDEX regional climate models over Australia: model performance and errors. *Climate Dynamics*, 52, 121–3005. Available from: <https://doi.org/10.1007/s00382-019-04672-w>
- Donmez, B., Donmez, K., Diren-Ustun, D.H. & Unal, Y. (2022) Urbanization-induced changes in convective and frontal precipitation events in Ankara. *Urban Climate*, 46, 101316.
- Evans, J.P., Di Virgilio, G., Hirsch, A.L., Hoffmann, P., Remedio, A.R., Ji, F. et al. (2021) The CORDEX-Australasia ensemble: evaluation and future projections. *Climate Dynamics*, 57, 1385–1401. Available from: <https://doi.org/10.1007/s00382-020-05459-0>
- Fan, J., Zhang, Y., Li, Z., Hu, J. & Rosenfeld, D. (2020) Urbanization-induced land and aerosol impacts on sea-breeze circulation and convective precipitation. *Atmospheric Chemistry and Physics*, 20, 14163–14182. Available from: <https://doi.org/10.5194/acp-20-1416three-2020>
- Freidenreich, S.M. & Ramaswamy, V. (1999) A new multiple-band solar radiative parameterization for general circulation models. *Journal of Geophysical Research*, 104, 31389–31409.
- Friedl, M. & Sulla-Menashe, D. (2015) *MCD12C1 MODIS/Terra+Aqua Land Cover Type Yearly L3 Global 0.05Deg CMG V006*. NASA EOSDIS Land Processes DAAC. <https://doi.org/10.5067/MODIS/MCD12C1.006>
- Friedl, M.A., Sulla-Menashe, D., Tan, B., Schneider, A., Ramankutty, N., Sibley, A. et al. (2010) MODIS collection 5 global land cover: algorithm refinements and characterization of new datasets. *Remote Sensing of Environment*, 114, 168–182.
- Georgescu, M., Broadbent, A.M., Wang, M., Krayenhoff, E.S. & Moustafaoui, M.J.E.R.L. (2021) Precipitation response to climate change and urban development over the continental United States. *Environmental Research Letters*, 16(4), 044001. Available from: <https://doi.org/10.1088/1748-9326/abd8ac>
- Grose, M.R., Moise, A.F., Timbal, B., Katzfey, J.J., Ekström, M. & Whetton, P.H. (2015) Climate projections for southern Australian cool-season rainfall: insights from a downscaling comparison. *Climate Research*, 62, 251–265.
- Han, J.Y., Baik, J.J. & Lee, H. (2014) Urban impacts on precipitation. *Asia-Pacific Journal of Atmospheric Sciences*, 50, 17–30. Available from: <https://doi.org/10.1007/s13143-014-0016-7>
- Hertwig, D., Ng, M., Grimmond, S., Vidale, P.L. & McGuire, P.C. (2021) High-resolution global climate simulations: representation of cities. *International Journal of Climatology*, 41, 3266–3285. Available from: <https://doi.org/10.1002/joc.7018>
- IPCC. (2022a) In: Shukla, P.R., Skea, J., Slade, R., Al Khourdajie, A., van Diemen, R., McCollum, D. et al. (Eds.) *Climate change 2022: mitigation of climate change*. Contribution of Working Group III to the Sixth Assessment Report of the Intergovernmental Panel on Climate Change. Cambridge, UK and New York, NY, USA: Cambridge University Press. Available from: <https://doi.org/10.1017/9781009157926>
- IPCC. (2022b) In: Pörtner, H.-O., Roberts, D.C., Tignor, M., Poloczanska, E.S., Mintenbeck, K., Alegria, A. et al. (Eds.) *Climate change 2022: impacts, adaptation and vulnerability. Contribution of working group II to the sixth assessment report of the intergovernmental panel on climate change*. Cambridge, UK and New York, NY, USA: Cambridge University Press. Cambridge University

- Press, p. 3056. Available from: <https://doi.org/10.1017/9781009325844>
- Katzfey, J., Schlünzen, H., Hoffmann, P. & Thatcher, M. (2020) How an urban parameterization affects a high-resolution global climate simulation. *Quarterly Journal of the Royal Meteorological Society*, 146, 3808–3829. Available from: <https://doi.org/10.1002/qj.3874>
- Katzfey, J.J., Nguyen, K.C., McGregor, J., Hoffmann, P., Ramasamy, S., Nguyen, H.T. et al. (2016) High-resolution projections for Vietnam - methodology and evaluation for current climate. *Asia-Pacific Journal of Atmospheric Sciences*, 52, 91–106. Available from: <https://doi.org/10.1007/s13143-016-0011-2>
- Kowalczyk, E.A., Wang, Y.P. & Law, R.M. (2006) *The CSIRO atmospheric biosphere land exchange (CABLE) model for use in climate models and as an offline model. Pap. 013*. Victoria, Australia: CSIRO Mar. and Atmos. Res., Aspendale. (Available at http://www.cmar.csiro.au/e-print/open/kowalczyke_a_2006a.pdf).
- Kusaka, H., Nishi, A., Mizunari, M. & Yokoyama, H. (2019) Urban impacts on the spatiotemporal pattern of short-duration convective precipitation in a coastal city adjacent to a mountain range. *Quarterly Journal of the Royal Meteorological Society*, 145, 2237–2254. Available from: <https://doi.org/10.1002/qj.3555>
- Lacis, A. & Hansen, J. (1974) A parameterization of the absorption of solar radiation in the Earth's atmosphere. *Journal of the Atmospheric Sciences*, 31, 118–133.
- Langendijk G.S., Halenka T., Hoffmann P., Adinolfi M., Campino A.A., Asselin O., Bastin S., Bechtel B., Belda M., Bushenkova A., Campanale A., Chun K.P., Constantinidou K., Coppola E., Demuzere M., Quang-Van D., Evans J., Feldmann H., Fita L., Gräwe D., Hadjinicolaou P., Hamdi R., Hundhausen M., Fernandez J., Johannsen F., Milovac J., Katragkou E., Kotlarski S., Le Roy B., Lemonsu A., Lennard C., Lipson M., Mandal S., Pabón L.E.M., Pavlidis V., Pietikäinen J.-P., Raffa M., Raluy-López E., Rechid D., Rui I., Schulz J.-P., Soares P.M.M., Takane Y., Teichmann C., Thatcher M., Top S., Van Schaeybroeck B., Wang F., Yuan J. (2024): Towards better understanding the urban environment and its interactions with regional climate change -the WCRP CORDEX flagship pilot study URB-RCC. Submitted to Urban Climate. Available at SSRN: <https://ssrn.com/abstract=&eqs;4846089> or <http://dx.doi.org/10.2139/ssrn.4846089>.
- Langendijk, G.S., Rechid, D. & Jacob, D. (2019) Urban Areas and Urban–Rural Contrasts under Climate Change: What Does the EURO-CORDEX Ensemble Tell Us?—Investigating near Surface Humidity in Berlin and Its Surroundings. *Atmosphere*, 10, 730. Available from: <https://doi.org/10.3390/atmos10120730>
- Lipson, M., Hart, M. & Thatcher, M. (2017) Efficiently modelling urban heat storage: an interface conduction scheme in an urban land surface model (aTEB v2.0). *Geoscientific Model Development*, 10, 991–1007.
- Lipson, M.J., Grimmond, S., Best, M., Abramowitz, G., Coutts, A., Tapper, N. et al. (2024) Evaluation of 30 urban land surface models in the urban-PLUMBER project: phase 1 results. *Quarterly Journal of the Royal Meteorological Society*, 150(758), 126–169. Available from: <https://doi.org/10.1002/qj.4589>
- Liu, J. & Niyogi, D. (2019) Meta-analysis of urbanization impact on rainfall modification. *Scientific Reports*, 9, 7301. Available from: <https://doi.org/10.1038/s41598-019-42494-2>
- Luhar, A.K., Thatcher, M. & Hurley, P.J. (2014) Evaluating a building-averaged urban surface scheme in an operational mesoscale model for flow and dispersion. *Atmospheric Environment*, 88, 47–58.
- Masson, V. (2000) A physically-based scheme for the urban energy budget in atmospheric models. *Boundary-layer Meteorology*, 94, 357–397.
- McGregor, J.L. (2003) A new convection scheme using a simple closure. *BMRC, Melbourne, Australia, Research Report*, 93, 33–36.
- McGregor, J.L. & Dix, M.R. (2008) An updated description of the conformal cubic atmospheric model. In: Hamilton, K. & Ohfuchi, W. (Eds.) *High-resolution simulation of the atmosphere and ocean*. New York, NY: Springer, pp. 51–76. https://doi.org/10.1007/978-0-387-49791-4_4
- Meinshausen, M., Smith, S.J., Calvin, K., Daniel, J.S., Kainuma, M., Lamarque, J.F. et al. (2011) The RCP greenhouse gas concentrations and their extensions from 1765 to 2300. *Climatic Change*, 109, 213–241.
- Minobe, S., Park, J.H. & Virts, K.S. (2020) Diurnal cycles of precipitation and lightning in the tropics observed by TRMM3G68, GSMap, LIS, and WWLLN. *Journal of Climate*, 33, 4293–4313. Available from: <https://doi.org/10.1175/JCLI-D-19-0389.1>
- Oke, T.R., Mills, G., Christen, A. & Voogt, J.A. (2017) *Urban Climates*. Cambridge: Cambridge University Press. Available from: <https://doi.org/10.1017/9781139016476>
- Oleson, K.W. & Feddema, J. (2020) Parameterization and surface data improvements and new capabilities for the community land model urban (CLMU). *Journal of Advances in Modeling Earth Systems*, 12, e2018MS001586. Available from: <https://doi.org/10.1029/2018MS001586>
- Paul, S., Ghosh, S., Mathew, M., Devanand, A., Karmakar, S. & Niyogi, D. (2018) Increased spatial variability and intensification of extreme monsoon rainfall due to urbanization. *Scientific Reports*, 8(1), 3918.
- Qian, Y., Chakraborty, T.C., Li, J., Li, D., He, C., Sarangi, C. et al. (2022) Urbanization impact on regional climate and extreme weather: current understanding, uncertainties, and future research directions. *Advances in Atmospheric Sciences*, 39, 819–860. Available from: <https://doi.org/10.1007/s00376-021-1371-9>
- Rotstayn, L.D. (1997) A physically based scheme for the treatment of stratiform clouds and precipitation in large-scale models. I: description and evaluation of the microphysical processes. *Quarterly Journal of the Royal Meteorological Society*, 123, 1227–1282.
- Rotstayn, L.D. & Lohmann, U. (2002) Simulation of the tropospheric sulfur cycle in a global model with a physically based cloud scheme. *Journal of Geophysical Research*, 107. AAC 20-1–AAC 20-21. Available from: <https://doi.org/10.1029/2002JD002128>
- Schlünzen, K.H., Hoffmann, P., Rosenhagen, G. & Riecke, W. (2010) Long-term changes and regional differences in temperature and precipitation in the metropolitan area of Hamburg. *International Journal of Climatology*, 30, 1121–1136. Available from: <https://doi.org/10.1002/joc.1968>
- Schwarzkopf, M.D. & Ramaswamy, V. (1999) Radiative effects of CH₄, N₂O, halocarbons and the foreign-broadened H₂O continuum: a GCM experiment. *Journal of Geophysical Research*, 104, 9467–9488.
- Shen, Y. & Yang, L. (2023) Divergent urban signatures in rainfall anomalies explained by pre-storm environment contrast. *Geophysical Research Letters*, 50, e2022GL101658. Available from: <https://doi.org/10.1029/2022GL101658>

- Thatcher, M. & Hurley, P. (2012) Simulating Australian urban climate in a mesoscale atmospheric numerical model. *Boundary-Layer Meteorology*, 142, 149–175.
- Thevakaran, A., McGregor, J.L., Katzfey, J., Hoffmann, P., Suppiah, R. & Sonnadara, D.U.J. (2016) An assessment of CSIRO conformal cubic atmospheric model simulations over Sri Lanka. *Climate Dynamics*, 46, 1861–1875. Available from: <https://doi.org/10.1007/s00382-015-2680-4>
- Watters, D., Battaglia, A. & Allan, R.P. (2021) The diurnal cycle of precipitation according to multiple decades of global satellite observations, three CMIP6 models, and the ECMWF reanalysis. *Journal of Climate*, 34, 5063–5080. Available from: <https://doi.org/10.1175/JCLI-D-20-0966.1>
- World Meteorological Organization (WMO). (2023) *Guidance on measuring, modelling and monitoring the canopy layer urban heat Island (CL-UHI)*, Vol. 1292. Geneva: WMO-No., p. pp88. https://library.wmo.int/index.php?lvl=notice_display&id=22236.
- Xiao, F., Zhu, B. & Zhu, T. (2021) Inconsistent urbanization effects on summer precipitation over the typical climate regions in

central and eastern China. *Theoretical and Applied Climatology*, 143, 73–85. Available from: <https://doi.org/10.1007/s00704-020-03404-z>

SUPPORTING INFORMATION

Additional supporting information can be found online in the Supporting Information section at the end of this article.

How to cite this article: Katzfey, J., Schlünzen, K.H. & Hoffmann, P. (2024) Effects of urban areas on the diurnal cycle of temperature and precipitation in a global climate simulation. *Quarterly Journal of the Royal Meteorological Society*, 150(765), 4885–4914. Available from: <https://doi.org/10.1002/qj.4847>